Simulation and Design Optimization for Linear Wave Phenomena on Metamaterials

by

Joel Saà-Seoane

Eng. Camins, Canals i Ports, UPC (2010)
Llic. Matemàtiques, UPC (2008)

Submitted to the School of Engineering
in partial fulfillment of the requirements for the degree of
Master of Science in Computation for Design and Optimization
at the
MASSACHUSETTS INSTITUTE OF TECHNOLOGY
June 2011

Author .....
Joel Saà-Seoane
School of Engineering
May 6, 2011

Certified by .....
Jaume Peraire
Professor of Aeronautics and Astronautics
Thesis Supervisor

Certified by .....
Ngoc-Cuong Nguyen
Research Scientist
Thesis Supervisor

Accepted by .....
Nicolas Hadjiconstantinou
Associate Professor of Mechanical Engineering
Director, Computation for Design and Optimization

Simulation and Design Optimization for Linear Wave Phenomena on Metamaterials

by

Joel Saà-Seoane

Submitted to the School of Engineering
on May 6, 2011, in partial fulfillment of the
requirements for the degree of
Master of Science in Computation for Design and Optimization

Abstract

Periodicity can change materials properties in a very unintuitive way. Many wave propagation phenomena, such as waveguides, light bending structures or frequency filters can be modeled through finite periodic structures designed using optimization techniques. Two different kind of problems can be found: those involving linear waves and those involving nonlinear waves. The former have been widely studied and analyzed within the last few years and many interesting results have been found: cloaking devices, superlensing, fiber optics The latter is a topic of high interest nowadays and a lot of work still needs to be done, since it is far more complicated and very little is known. Nonlinear wave phenomena include acoustic amplitude filters, sound bullets or elastic shock mitigation structures, among others.

The wave equation can be solved accurately using the Hybridizable Discontinuous Galerkin Method both in time and in frequency domain. Furthermore, convex optimization techniques can be used to obtain the desired material properties. Thus, the path to follow is to implement a wave phenomena simulator in 1 and 2 dimensions and then formulate specific optimization problems that will lead to materials with some particular and special properties. Within the optimization problems that can be found, there are eigenvalue optimization problems as well as more general optimal control topology optimization problems.

This thesis is focused on linear phenomena. An HDG simulation code has been developed and optimization problems for the design of some model devices have also been formulated. A series of numerical results are also included showing how effective and unintuitive such designs are.

Thesis Supervisor: Jaume Peraire
Title: Professor of Aeronautics and Astronautics

Thesis Supervisor: Ngoc-Cuong Nguyen
Title: Research Scientist

Acknowledgments

Let me first of all thank the 'La Caixa' fellowship program, which has really allowed me to come to MIT. Not only has it provided me with all the expenses for this experience but also has given me the chance of living this fantastic experience as well as of meeting great fellows from many different fields. I really feel privileged, lucky and fortunate for having been awarded with such a prestigious fellowship.

This thesis would have not been possible without the constant help of my advisor and thesis supervisor, Professor Jaume Peraire. His patience, effort and continuous help as well as motivation have lead me into the world of Research in a much easier way. He is always been looking for new approaches, thinking on new possible applications and linking all this research with many projects out there which are of real interest for this society. The work has been much less heavier with his guidance and I am very grateful for that.

Dr. Cuong Nguyen has also been continuously working on this project and his contributions are nothing but essential. Whenever I needed any kind of advice or guidance he was there, at any time, any day. It has been a great pleasure having the chance of working head to head with him and learning so much from all his knowledge. Professor Robert M. Freund has also been involved in this project since the very beginning and his always clever ideas have pushed the optimization forward. Professor Pablo Parrilo and Dr. Abby Men have also been a source of inspiration for this whole project with their joint work on Photonic Bandgap Optimization together with Prof. Peraire, Prof. Freund and Dr. Nguyen.

I would also like to thank David Moro for being a very pleasant fellow traveller. Together with Carmen Guerra they have been great friends with whom to share any concern in this american adventure. Hemant Chaurasia and Andrew March have also been very helpful when preparing quals and in many other situations and I also want to extent my gratefulness to all the ACDL labmates. I do not want to miss the permanent help provided by Laura Koller and Jean Sofronas regarding any academic and professional issues. I would also like to extend my gratefulness to my 'La Caixa'

fellows in the Boston area and all the other friends here for all the good and not so good moments.

However I would not be here if it wasn't because of all my previous experiences in Barcelona. Professor Antonio Huerta and especially Professor M. Rosa Estela have always encouraged me to come and helped me in zillions of ways. Their experience and pieces of advice have been the key point of being here and up to the point that they are now good friends of mine.

Last but clearly not least, my family and friends. Although I will never regret, it was hard to leave everything behind and come alone to Cambridge, MA, especially after arriving in this new world on a freezing January friday evening. Both Mum and Dad, as well as my brother Raul have always been there for any problem I could have. The over 3600 miles between Barcelona and Cambridge would not even be close to make us lose contact or even weaken how much we worry about each other. And Cris, your daily patience, advice and understanding has made it much easier. A huge part of this is really thanks to you. It has been difficult to cope with such a distance all this time and so it will be, but be optimistic, you know we will get it.

Contents

List of Figures

List of Tables

Chapter 1

Introduction

From ancient ages it has always been a human skill to take advantage of materials that have proven its usefulness. Since the very beginning, our ancestors knew that sharpened stones would make hunting a much easier task. Thanks to those materials found on the Earth we have been able to design and build tools without which we couldn't now live. However, material science has evolved much more than may be thought.

At some point in history (around 4,000 years ago) brilliant minds noted that manipulating natural materials appropriately one could obtain much better *special* properties from them. For instance, we can think of steel as a clever combination of iron and a little bit of some alloying material (commonly carbon but many other metals can be considered) which leads to a new material with much improved mechanical properties than iron.

More recently, attention has focused on electric and optical properties of materials. From these considerations superconductors, fiber optics, waveguides and many more advanced materials have been designed and are topics of active research in the current days.

The next step in this field focuses on the design of *metamaterials*. Metamaterials are basically artificially designed materials that have a very specific microscopic structure such that the macroscopic behavior of such material is one that can not be achieved using homogeneous natural materials (or a macroscopic combination of

them). The macroscopic properties are acquired because of the microscopic structure (usually a periodically repeated pattern) more than by the composition itself, so steel would not be a metamaterial. Examples of metamaterials would be materials with negative index of refraction, in optics, or negative Poisson's ratio, in mechanics, among many others that will be discussed later on in this thesis.

The work that we have been carrying out within the last few months tries to provide a simulation tool for linear metamaterials and some optimized macroscopic devices providing certain complex properties. This thesis tries to summarize the work done on this field and will be therefore structured in five chapters:

- The first chapter gives the motivation for this work as well as an introduction to the simulation and optimization tools that have been considered and developed;
- The second chapter describes the Hybridizable Discontinuous Galerkin method developed for the wave equation;
- The third introduces the optimization problems as well as the techniques used to solve them;
- The fourth chapter presents some numerical results that have been obtained from this work; and,
- The last chapter summarizes the main conclusions and highlights some future research, including nonlinear problems and robust optimization.

This topic is nowadays a very active field of research and the number of scientific publications has grown exponentially over the last years. It is likely that in a few years most of the metamaterials analyzed here and many more will be a reality in everyday lives and very likely they will completely change social patterns, once more.

1.1 Motivations for metamaterials' design

Let's introduce the idea of metamaterials through two examples: the photonic bandgap wave phenomena in $2d$ and the negative Poisson's ratio materials for linear elasticity.

1.1.1 Photonic Bandgap in $2d$

We consider the wave propagation pattern in a given media[1]. If we fix this reference media to be, for example, air, and we consider a point source at the left side of the boundary, the propagation pattern is shown in figure 1-1. However, if we now include some randomly placed rods of a different material, say some silicon with different properties[2] than the reference air, the propagation pattern changes. In fact, we could analytically derive the interaction between the reflected and transmitted waves and obtain an expression for the total wave field. Nevertheless, we can already see in figure 1-2 that the new pattern looks quite random, especially if we are close to the rods.

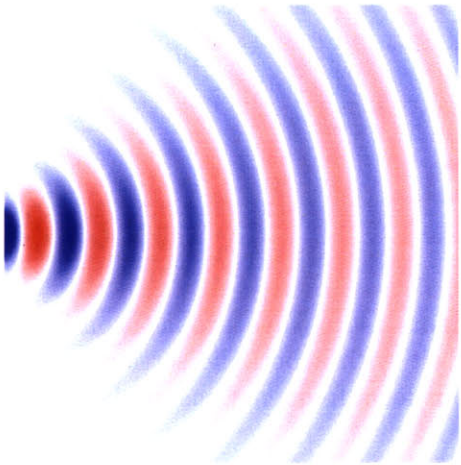

Figure 1-1: Wave propagation pattern in air

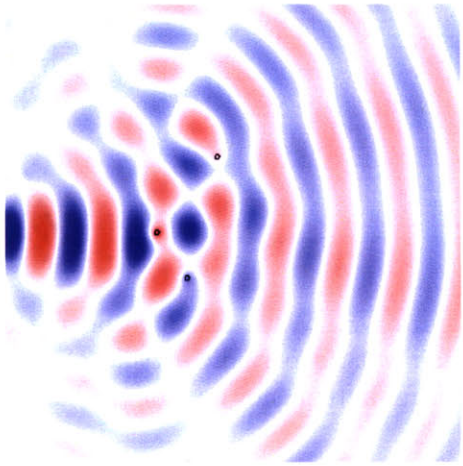

Figure 1-2: Wave propagation pattern in air with three silicon rods

The most interesting results show up when considering a periodic distribution of the silicon rods. As we see in figure 1-3 the propagated field turns up to be organized and coherent. That is, if the rods are periodically distributed, the amplitude of the resulting wave is coherent and not unstructured as in the case of the three randomly set rods anymore. This very interesting result is actually not hard to understand from

[1]This simulations have been run using the free Software Meep [42] developed at MIT by Steven G. Johnson et al. This section has also been inspired in his motivation lecture for the course 18.369-Mathematical methods in Nanophotonics, also at MIT.

[2]Such different properties will be further defined for each problem whenever they are simulated or optimized in forthcoming chapters.

the fact that, due to the inner symmetries of the material (hexagonal or triangular in this case) the transmitted and/or reflected waves interact in a way such that all propagations cancel out except from the very organized one. This is only true however for certain frequencies and in fact, if we tune a little bit that frequency up (just increase it by a 20%) the propagation pattern changes completely and everything is now reflected, as shown in figure 1-4. This phenomena is called bandgap and will be further described in chapters 3 and 4.

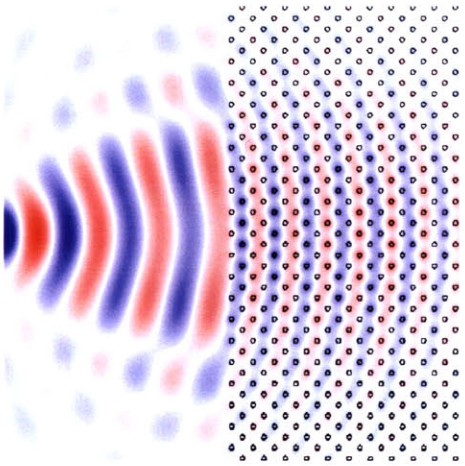

Figure 1-3: Wave propagation pattern in air with a periodic setting of silicon rods for a frequency outside the bandgap

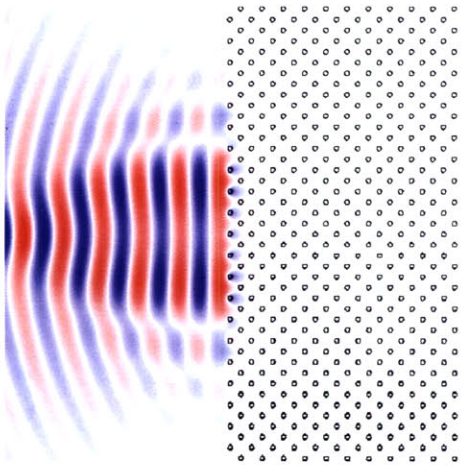

Figure 1-4: Wave propagation pattern in air with a periodic setting of silicon rods for a frequency inside the bandgap

This bandgap phenomena makes us think of some optimization problems such as: what is the optimal rod distribution so that we can maximize the range of frequencies that fit in the bandgap? Or more generally, how is the pattern (not necessarily rods) such that we can maximize that range? This questions have been nicely answered in [27] for an infinitely periodic distribution of the pattern. This is very remarkable from a theoretic point of view but does not answer all the important questions from a practical perspective. It is actually one of the motivations of the work presented in this thesis and one of the novelties that are offered here: simulations have been run assuming finiteness of the pattern and therefore boundary interactions. Thanks to that, the structures obtained here are more realistic and closer to be manufacturable.

Furthermore, the existence of such range where there is no propagation is the

basis for many practical devices. For instance waveguides, which consider a linear defect in the triangular distribution of rods throughout which the wave propagates but always exponentially decays out of it (within the rod distribution). This leads to high efficient wave conduction (fiber optics...). Figures 1-5 and 1-6 show how we can easily create a waveguide. Thinking a little bit further we can create efficient wave bends (see [50]) as shown in figure 1-7.

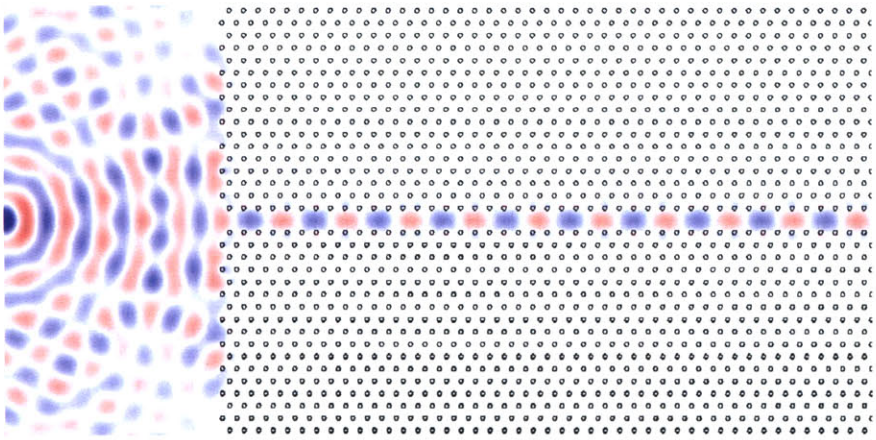

Figure 1-5: Wave propagation pattern within a waveguide of air on a periodic setting of silicon rods for a frequency inside the bandgap

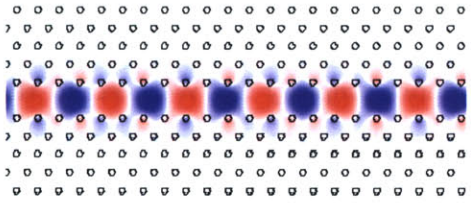

Figure 1-6: Waveguide propagation pattern on a hexagonal lattice

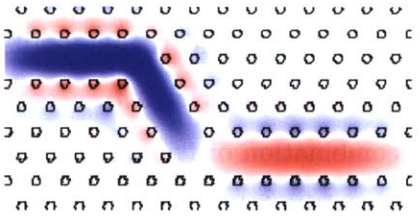

Figure 1-7: Waveguide bend propagation pattern on a hexagonal lattice

1.1.2 Negative Poisson's ratio in Linear elasticity

One very desired property of a material is to be auxetic, i.e. provide a negative Poisson ratio, that is a material that widens up under stretching, instead of getting thinner. This particular behavior is not provided directly by any material that one

can find in the nature and therefore it will be called a metamaterial. The macroscopic property observed, also called effective, can certainly give very special values.

Back in 1987, it was firstly introduced by Lakes in [24] that materials exhibiting a negative Poisson's ratio could be developed. Such materials will expand laterally when stretched and, reversely, contract laterally when compressed. Such unusual property is achieved by forming cells into a so-called 're-entrant' shape which unfolds and expands in one direction when a positive tension is applied in the orthogonal direction.

Different microstructural patterns might lead to an effective negative Poisson's ratio. We always look for structures that are, somehow, folded in a way such that after tension, even if the material itself contracts laterally due to a positive internal Poisson's ratio, the global picture of the structure unfolds and thus widens up. Some possible configurations were introduced and analyzed in [25]. It has been observed that some effective patterns come from inverted hexagonal honeycombs. These kind of structures have also been analyzed in [13, 55, 56], for instance, and conforms the state-of-the-art research in this field. An extension of the work presented here can be found in [51].

If we want to achieve an effective global negative Poisson's ratio for a certain macroscopic material thanks to its microscopic structure we need to think about how such particular structure providing the global property is. We need to think of a combination of two materials[3] (E, ν) and (E', ν') considered in a way that it is because of its interaction that we obtain widening under stretching. For simplicity and without loss of generality let's just consider that one reference material is air[4] and let's characterize the other by (E, ν).

Figure 1-8 shows the configuration that will be considered. In fact the outer region is going to be made of the reference elastic material whereas the inner bow tie region is considered to be the deformable solid or just air. What a negative Poisson's ratio

[3]Different materials meaning different Young's modulus E and different Poisson's ratio $\nu > 0$, basically one large E and the other not so large.

[4]Note that air is not actually a solid and thus the Young's modulus does not apply. Consider equivalently the bulk modulus or just take very deformable solid ($E \sim 0$).

formally means is that the transversal strain has the same sign as the longitudinal strain, i.e. stretching in a given direction implies expansion in the orthogonal space of such direction, or reversely. Classic isotropic materials, and by classic one must read findable in nature, the Poisson's ratio can take values from very close to zero for cork[5] or certain foams and up close to 0.5 for certain clays, gold and rubber[6].

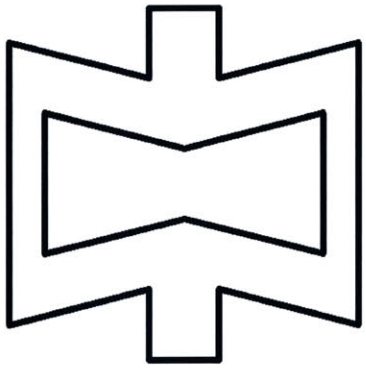

Figure 1-8: Inverted Hexagonal Honeycomb setting, one basis element.

The boundary conditions play an important role. Both the horizontal displacement at the leftmost side of the domain and the vertical displacement of the bottom-most nodes are pinned. Furthermore, an uniform force on the right boundary needs to be considered. Figure 1-9 shows the boundary conditions used for this problem.

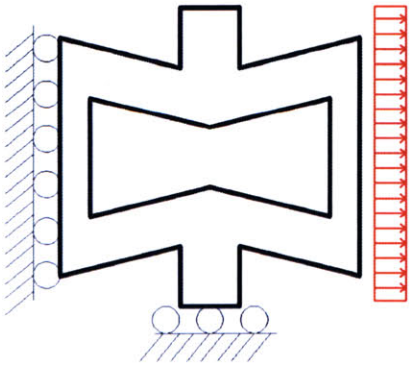

Figure 1-9: Boundary conditions for the reference element under x stresses.

[5]That's the reason why it is used as a stopper for wine bottles!
[6]Note $\nu = 0.5$ corresponds to the incompressible limit and no volume changes

First of all let's solve the problem on a quarter of the element. The effective Poisson's ratio obtained for this case is $\nu_{11} = -0.48$ and figure 1-10-top-left shows the deformed structure. The contours show the displacements in the y direction whereas the displacements in the orthogonal direction can be shown in the inset together with a shadow of the initial configuration to be compared with the deformed one.

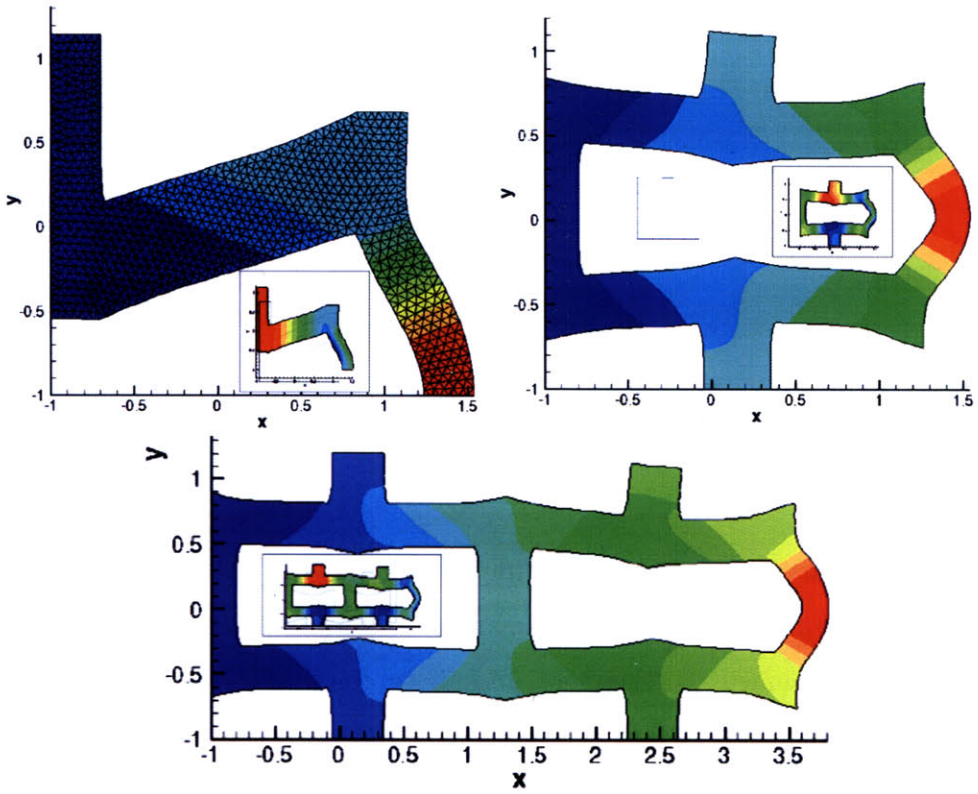

Figure 1-10: Top-left: Displacements for the quarter element. Mesh and contours for d_y are shown in the main figure. The inset shows contours in x and initial configuration. Top-right: same for the 1×1 lattice of elements. Insets show initial configuration and orthogonal displacements. Bottom: same but for a 1×2 elements setting.

Similarly figure 1-10-top-right shows the same situation for the one by one elements lattice. The value that the Poisson's ratio attains for this case is $\nu = -0.37$. Furthermore, figure 1-10-bottom shows the one by two elements lattice structure which provides a Poisson's ratio of $\nu = -0.36$. Finally, figure 1-11-left shows the displacement field in x for the two by two element lattice. The Poisson's ratio for this

case takes a value of $\nu = -0.36$ once more. The right hand side of the same figure defines a ten by ten elements lattice which shows how the microscopical structure of the macroscopical material would look like.

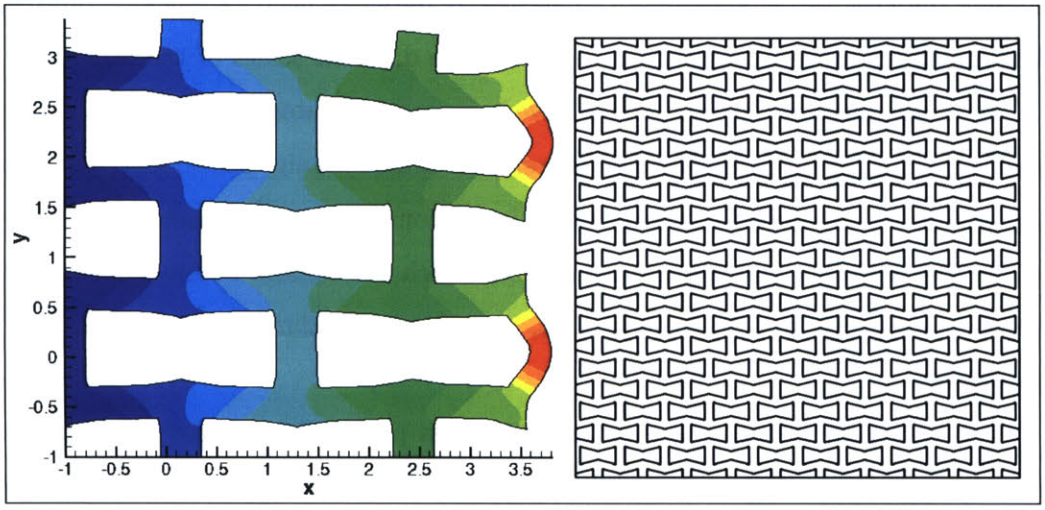

Figure 1-11: Left: Displacements for the two by two elements lattice. Right: ten translational periods in both x and y.

1.2 Simulating metamaterials

Metamaterials are microscopic combinations of materials with different properties that end up giving a very specific macroscopic property or behavior. The phenomena that we would like to model are defined by a governing equation which will be a Partial Differential Equation, often the Wave Equation. There are many numerical methods to simulate PDE-governed problems that can be found in the literature but in our particular case heterogeneous materials are to be considered and therefore such numerical methods will be required some further capabilities. It is therefore essential to focus our attention on numerical methods with improved accuracy and efficiency for solving acoustic, elastic and electromagnetic wave equations in heterogeneous media.

Accurate numerical simulation of wave propagation in metamaterials present several challenges. To begin with, metamaterials are always heterogeneous media con-

sisting of a host material (often air) embedded with several hundreds or thousands of small inclusions of another material (often silicon). As in [19], sometimes a repeated pattern is obtained and the periodicity of such patterns can have sizes considerably smaller than the actual wavelength. This clearly implies a need for efficient, multiscale and scalable numerical algorithms to resolve the different scales of the problem.

Secondly, most of the simulations have been run for materials which have been derived through physical intuition and therefore assumed infinite periodicity, i.e. boundary conditions are periodic, which make simulations a great deal easier. However, we would like to design manufacturable devices which can seldom be modeled as having infinite periodicity and because of that, absorbing boundary conditions need to be considered.

It is also very common to require that waves propagate over long distances and over many periods. High-order accurate methods are thus needed to control numerical dispersion and dissipation errors.

Another frequent issue appears since most problems of practical interest will involve complex geometries and very sharp and strong contrasts in wave speeds throughout the heterogeneous media. This will require adaptive mesh refinement to accurately represent the geometry.

And finally, last but not least, one of the most serious challenges is that nonlinear wave propagation may give rise to discontinuities and shock waves. This requires shock-capturing algorithms to be developed for computing stable and sharp shock profiles. Although nonlinear wave propagation is not considered in this thesis, it is one of the main aims of our future research.

The simulation methods considered here are based on previously developed methods that can be found in [31, 32, 35, 36, 37, 38, 39, 40, 41].

1.2.1 The Wave and Helmholtz Equations

The wave equation is a second order hyperbolic partial differential equation that models the propagation of waves. This particular PDE arises in acoustics, elasticity or electromagnetism and defines the governing equation for most of the problems that

we are interested in. Figure 1-12 shows the spectrum where the wave equation acts as a governing equation in terms of the wavelength or, equivalently, the frequency. In its simplest scalar form, the wave equation is written as[7] follows:

$$\frac{\partial^2 u}{\partial t^2} - c^2 \nabla^2 u = 0 \tag{1.1}$$

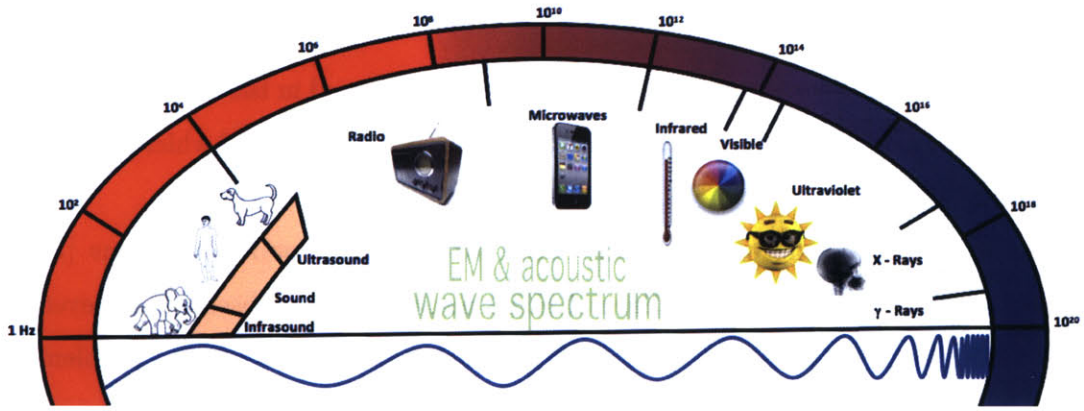

Figure 1-12: Wave phenomena spectrum: Electromagnetic and Acoustic wave scales.

Note that c is defined as the wave propagation speed for a given media. This wave equation can be reduced to the so called Helmholtz equation when frequency domain is considered. In fact, when dealing with any linear phenomena there is no reason for considering the full time and space dependent equation since the time dependance can be eliminated by expressing the solution as a superposition of simple oscillatory solutions. All linear problems considered here do not have a time evolution and problems will be reduced to the Helmholtz equation.

We consider (1.1) and a solution of it of the form $U(x,t) = u(x)T(t)$ where $T(t) = e^{i\omega t}$ for some given frequency ω. Inserting this form of the solution into equation (1.1) we obtain:

$$\frac{\partial^2 U}{\partial t^2} - c^2 \nabla^2 U = 0 \quad \Leftrightarrow \quad u(x)(i\omega)^2 e^{i\omega t} - c^2 \nabla^2 u(x) e^{i\omega t} = 0 \tag{1.2}$$

[7]Note that since it is a hyperbolic equation initial conditions need to be provided as well as either left or right hand side boundary conditions. Depending on each particular problem (wave propagation speed greater or smaller than sound/light speed) we might need all boundary conditions or just some of them

Thus we can finally write the Helmholtz equation as

$$\nabla^2 u(x) + k^2 u(x) = 0 \tag{1.3}$$

where $k = \omega/c$.

1.3 The simulation tools

The simulation tools that are presented, developed and used in the context of this thesis are based on the a Hybridizable Discontinuous Galerkin Method which is described in a series of recent papers: [31, 32, 33, 34, 35, 36, 37, 38, 39, 40, 41].

The first HDG method was introduced for diffusion-reaction problems [7] and later analyzed in [3, 8, 9, 10]. Several HDG methods were subsequently developed for biharmonic equations [4], linear and nonlinear convection-diffusion problems [5, 34, 33], linear elasticity [52], Stokes flows [35, 36], compressible and incompressible Navier-Stokes equations [46] and also time-harmonic Maxwell equations [41].

1.4 Optimizing metamaterials

The simulation of wave propagation phenomena in metamaterials requires the solution of complex Partial Differential Equations for specific structures. In the design setting, however, one wishes to know the answer to the question: which pattern or configuration leads to optimal performance in terms of a given objective function? That is, say you want to design a cloaking device, then we not only need to be able to simulate a given configuration and composition of the cloak device, but also, and even more important, we need to find an optimal solution to such problem, i.e. a certain material composition that minimizes the difference between the output wave and what the output would be without any object in between. This question can be rigorously addressed by formulating optimization problems for the different cases considered. One of the main purposes of this thesis is to provide effective computational approaches for solving some linear metamaterial optimization problems.

We consider two types of optimization problems: the eigenvalue optimization problems and the optimal control ones. Some very efficient approaches to the eigenvalue optimization for the photonic bandgap maximization can be found in [27, 28]. Here we will focus mainly on the optimal control problems which are formulated as the minimization of a certain cost function (often minimize the L^2 distance from the current output to the desired one) subject to combined PDE based constraints and other linear and/or box constraints.

Some classical algorithms will be used to solve the optimization problems: sensitivities will be obtained based on a dual or lagrangian formulation in order to obtain the adjoint and then a classic gradient descent method will be used. Furthermore, some other new approaches will be formulated and introduced for future lines of research. Semi-definite programing (SDP) techniques have also been used to solve some of the problems considered as in [27, 28].

1.4.1 Classical approach

Most of the work on optimization for the design of metamaterials to date has been done using phisical intuition, due to the difficulties that the optimization problems show, and some impressive results have been reported. For example, it can be physically understood (see [19]) that if we want to maximize the photonic bandgap in a 2d structure for the transverse magnetic configuration, the introduction of non connected rods of silicon in air can produce a large band gap. Then we can optimize over the radius of the rods and the material properties, which are two parameters, and find the optimal distribution. Very remarkable results have been found using this kind of optimization as can be seen in [27, 28] for example.

However, a more sophisticated optimization can lead to a much better solution as we can see in figure 1-13. In this case an eigenvalue optimization problem has been formulated and solved using SDP techniques. This more sophisticated method has lead to much better results than the naive optimization by paying the price of solving a much harder optimization problem. However, both the naive optimization described above and the eigenvalue optimization have been particularly successful for

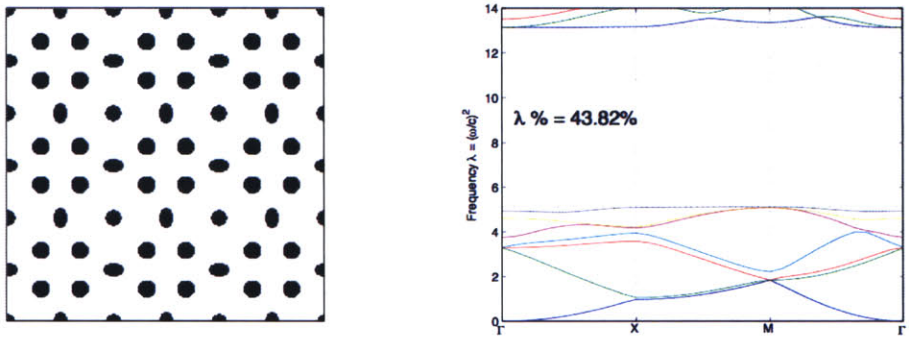

Figure 1-13: Optimal distribution for the TM bandgap maximization found in [27] and dispersion relation with bandgap-midgap ratio.

this problem of maximizing the bandgap-midgap ratio for either the transverse electric or transverse magnetic configuration on a 2d photonic crystal. It is not obvious that these approaches will be successful when we go to other types of applications.

All in all, here we are interested in formulating optimal control type problems in which we formulate an objective function and have a governing equation as a constraint as well as possible box and volume constraints. So the optimization problems that we are about to consider are of the form of equation (1.4).

$$\begin{aligned} \min_{\alpha,u} \quad & ||u - \bar{u}||^2 \\ \text{s.t.} \quad & \mathcal{F}(\alpha, u) = f \\ & \alpha_{min} \leq \alpha \leq \alpha_{max} \\ & \int_V \alpha \, dV \leq \xi \end{aligned} \tag{1.4}$$

Note that the volume constraint can also be pushed upwards into the objective function by duality in order to minimize the volume of a given material, if desired. Actually, since our problems will often have plenty of solutions and we are interested in the simplest one, we will force it to give the solution with smallest volume of such

material. The problem in that case will be written as in equation (1.5).

$$\begin{aligned} \min_{\alpha,u} \quad & ||u-\bar{u}||^2 + \varphi \int_V \alpha dV \\ \text{s.t.} \quad & \mathcal{F}(\alpha,u) = f \\ & \alpha_{min} \leq \alpha \leq \alpha_{max} \end{aligned} \tag{1.5}$$

This optimization problem can be very complicated to solve due to the governing equation itself, which can lead to a highly nonconvex objective function. The classical approach to be used will be based on formulating a dual-adjoint problem pushing the governing equation up into the objective function and then computing the gradients with respect to the design variables. A key point will be to find the best stepsize to move in the opposite direction of the computed gradient such that we minimize the objective but still satisfying the box constraints. This method has been analyzed and developed for the optimization problems that have been solved in the context of this thesis and can be further found in chapter 3. Due to the difficulties of the former optimization problems some new methodologies have been considered and will be one of the main future lines of research.

1.4.2 Main difficulties

The main point of this section is to highlight some of the main issues that need to be faced when dealing with the optimization formulations that show up in the context of this thesis. Firstly, note that the governing equation comes from a linear PDE. Thus, one might think that $\mathcal{F}(\alpha,u)$ in equations (1.4) and (1.5) represents a linear system of equations. However, sadly that is not the case, since even though the governing equation is linear in the state variables u, the design variables might appear multiplying the state or their derivatives.

Furthermore and for the same reason, the objective function is not really quadratic, even though it might look like that at first glimpse. That is because the state variables u depend on the design variables α and their relation is given by the nonlinear system of equations $\mathcal{F}(\alpha,u) = f$. Note that the volume constraint in (1.4) or the

corresponding term in the objective function in equation (1.5) is never going to be a problem since, in the first case, it is just a projection of the solution (or a renormalization of it) and, in the second case it is the classical dualization through Lagrange multiplyiers of a linear constraint.

Finally, the box constraints are going to be the largest source of difficulty. The formulations of either equation (1.4) or equation (1.5) are a relaxed version of what we really look for, which is $\alpha \in \partial([\alpha_{min}, \alpha_{max}]^n)$ if n is the length of α. That is, we want the vector of design variables to, pixel by pixel[8], either decide if it picks material A (which has $\alpha = \alpha_{min}$) or material B (which is $\alpha = \alpha_{max}$).

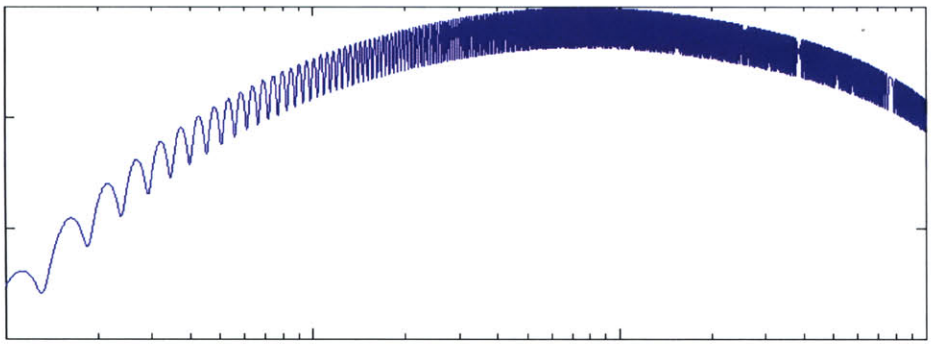

Figure 1-14: Possible objective function to maximize. Note that gradients would give directions totally useless if we seek to find the global maxima. Axis have been ignored.

To sum up, the solutions to optimization problems will always need to be considered as local minima (hopefully close enough to global optima). The nonlinearities globally found in both the governing equation and then in the objective function will lead to highly nonconvex objective functions, which needs to be taken into account. Gradients are at times useless since do not tell any information about global optima due to the local oscillations. Figure 1-14 shows a possible objective function where the global maxima will be very hard to find using the classic gradient, since these will always lead to any random local minima and get stuck there. Some methods based on smoothing the solution before considering the gradients will need to be considered.

[8]The reader should understand, here and on, an element of the discretization by the term pixel.

1.5 Some examples of Linear Problems

The simulation and optimization of metamaterials appears to be an important problem. That is the reason why this thesis tries to focus on some linear phenomena. The nonlinear phenomena, although of obvious interest, is outside the scope of this thesis due to its inherent complexity.

Moreover, although some of the linear phenomena have been widely studied, the perspective from which the optimization is carried out here is quite new and tries to be one of the main contributions of this thesis. The tools developed and the adapted code for the simulation of these linear phenomena are another of the contributions of this work.

The literature of simulation of linear wave phenomena gives a lot of examples, some of which will also be simulated here. Most of the optimization that has been found is efficient although quite naive and thus very problem dependent. In the linear regime, some interesting applications are related to photonics: Waveguides, wavebends, frequency filters, cloaking devices, superlensing, cavities... Nevertheless, most of these phenomena can be easily extended to other wave propagation problems outside electromagnetics. If we consider macrowave radio frequencies or even acoustic waves, the same principles would apply, but in these cases the real devices would have much larger dimensions. Other types of problems such some elasticity phenomena could also be modeled, such as negative Poisson's ratio materials... If we also considered the nonlinear phenomena, this variety of problems could be largely extended with elastic waves dispersion devices, sound bullets, acoustic amplitude earplugs... See, for instance, [15, 53] for some examples.

Chapter 2

The Hybridizable Discontinuous Galerkin Method for the wave equation

The hybridizable Discontinuous Galerkin Method is a new emerging DG approach firstly introduced by Cockburn, Gopalakrishnan and Lazarov in 2009 [7] and further analyzed and developed by Cockburn, Nguyen and Peraire in [31, 32, 35, 36, 37, 38, 39, 40, 41]. This method generalizes the classic Discontinuous Galerkin methods by introducing hybrid variables that decouple the interaction between different elements. Having considered that, local elemental problems can be very efficiently solved and then a reduced global problem is solved to find the final solution. This method has been very recently developed and shows very attractive properties such as the superconvergence that will be discussed at the end of this chapter.

2.1 HDG versus classic Finite Element Methods

The basic and key idea of the hybrid DG approach stands on introducing new variables on the edges called the numerical traces, which become the globally coupled variables of the problem. The numerical fluxes for the elemental problems are defined in terms of the traces and involve an additional stabilization parameter τ. In the end, these

new variables are such that decouple the interaction among neighboring elements and thus, the problem can be locally solved very efficiently. At the end, a global problem is solved for these new variables. It must be said that this new set of variables is much smaller (especially when going to high order polynomial approximation spaces) than the original set of DG variables since they are only defined on the edges. So we end up solving a number of inexpensive local problems and just one global problem for variables which are defined only on the edges and therefore is cheaper than a globally coupled DG.

The Finite Element Method has been a popular method to perform the spatial discretizations of wave propagation problems given its ability to handle complex geometries and inhomogeneous materials. This last property is of particular interest here. Using Finite Differences would not offer the desired flexibility for complicated geometries. Furthermore, Finite Volumes methods are not very suitable when high-order is desired. It must be said, though, that the HDG adapted method for the wave equation shares a lot of features with FV methods since both methods are formulated for systems of conservation laws. Boundary Integral methods would also be possible but their dense matrices as well as the difficulties to handle non-homogeneous materials and the limitation to linear problems have been considered to be too restrictive.

Once the FE method has been chosen there are still several spatial discretization strategies that can be considered. They include continuous Galerkin/Petrov-Galerkin methods, spectral element methods, mixed finite element methods, extended finite element methods and finally discontinuous Galerkin/Petrov-Galerkin methods. They could all have been used and they all have their strengths and weaknesses. However, due to its ability to combine complex geometry and high order solutions the Discontinuous Galerkin Finite Element methods, seem to be most suitable. They also offer stability and low dispersion for discretizations of hyperbolic systems, allow for a simple imposition of boundary conditions and are very flexible to future parallelization and adaptivity.

Clearly not everything are advantages with DG and thus one of the main drawbacks is due to the duplication of nodal degrees of freedom at the element boundary

interfaces. This deficiency is compensated in the HDG method since block diagonal systems of equations can be very efficiently solved in a local sense (only need to invert local matrices which are small).

Apart from that, time dependent problems will require time integration which can be carried out either using the well-known class of Newmark-finite element methods or just transforming all higher order time dependent semidiscretized PDEs into first order systems of ODEs that can be efficiently time integrated using either a backwards difference scheme or a Runge-Kutta, see [40] . However, since we only worry about linear phenomena and time dependance will be relaxed, there is no further analysis in this thesis.

2.2 The Helmholtz equation

Within this thesis, the adaptation of a class of hybridizable Discontinuous Galerkin methods (HDG) to the Helmholtz equation is firstly introduced. We want to numerically solve the first-order formulation of the acoustic, elastic and electromagnetic wave equation.

The HDG method has already been introduced for the linear and nonlinear convection diffusion equations by Nguyen, Peraire and Cockburn in [34] and [33] respectively, and here it has been adapted to the second order Helmholtz equation. As it is typical for the HDG methods, in order to carry out the discretization in space we basically proceed in two main steps. First of all, we formulate and solve the local problems where the approximate scalar variable and flux are expressed in an element-by-element fashion in terms of an approximate trace of the scalar variable along the element boundary. Then, we formulate and solve the global problem which is just obtaining a unique value for the trace at the inter-element boundaries by enforcing flux continuity. Figure 2-1 shows the extra degrees of freedom considered in the HDG versus the classical DG variables. Note that they are all on the boundaries and they are used to decouple all local problems and are then obtained by solving the global problem.

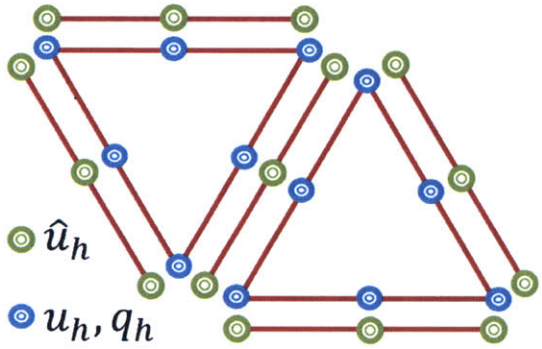

Figure 2-1: Degrees of freedom distribution for the described HDG method

Consider now the Helmholtz equation, where $\Omega \in \mathbb{R}^n$ represents the physical domain with boundary $\partial\Omega$. Then the strong formulation of the Helmholtz equation is the one in (2.1).

$$\begin{aligned} \nabla \cdot (\nabla u) + k^2 u = 0, \quad & \text{in } \Omega \\ u = g_D. \quad & \text{on } \Gamma_D \\ -\nabla u \cdot \mathbf{n} = g_N, \quad & \text{on } \Gamma_N \end{aligned} \tag{2.1}$$

where $k = \omega/c$ is the wavenumber or wavevector computed as the quotient between the frequency and the propagation speed of the media. Γ_D and Γ_N are the parts of the boundary where Dirichlet and Neumann boundary conditons are applied, respectively. They are such that $\bar{\Gamma}_D \cup \bar{\Gamma}_N = \partial\Omega$ and $\Gamma_D \cap \Gamma_N = \emptyset$.

2.3 HDG formulation

First we need to rewrite our problem (2.1) as a first order system of equations. That is, let's consider $\mathbf{q} = -\nabla u$ as an auxiliary variable that will correspond to the gradient of the displacement. With that we obtain equation (2.2).

$$\begin{aligned} \mathbf{q} + \nabla u = 0 \quad & \text{in } \Omega \\ -\nabla \cdot \mathbf{q} + k^2 u = 0, \quad & \text{in } \Omega \\ u = g_D. \quad & \text{on } \Gamma_D \\ \mathbf{q} \cdot \mathbf{n} = g_N, \quad & \text{on } \Gamma_N \end{aligned} \tag{2.2}$$

2.3.1 Notation

Let $\mathcal{T}_h$ be such that $\mathcal{T}_h = \bigcup_{i=1}^{n} K_i$[1] and $\mu_d(K_i \cap K_j) = \delta_{ij}$[2] where $dim(\Omega) = d$, that is, the intersection of two different elements of $\mathcal{T}_h$ (also called discretization space) only contains, at most, edges or interfaces and never elements. If $dim(\Omega) = d$, such intersection can only be, at most, of dimension $d-1$. In fact, if $\mu_{d-1}(K_i \cap K_j) \neq 0$ it means that K_i and K_j are neighbors and therefore we define their common interface or edge as $e_{ij}^o = K_i \cap K_j = \partial K_i \cap \partial K_j$ and it will be an interior interface or edge. The set of interior edges or interfaces is denoted as $\mathcal{E}_h^o$. Moreover, the set of elements such that $\mu_{d-1}(K_i \cap \partial\Omega) \neq 0$ are elements with an edge on the boundary and hence we define such edges through $e_i^\partial = K_i \cap \partial\Omega = \partial K_i \cap \partial\Omega$ and we put them all in a set called $\mathcal{E}_h^\partial$. Let's thus call $\mathcal{E}_h = \mathcal{E}_h^\partial \cup \mathcal{E}_h^o$.

Furthermore, the averages $\{\{\cdot\}\}$ and the jumps $[\![\cdot]\!]$ on the interior interfaces or edges need still be defined. Consider two neighboring elements and their common edge. Let then $(\mathbf{q}^+, u^+)$ be the values of the gradient (vector) and displacement (scalar) on the edge considered as an edge of one of the two elements, and $(\mathbf{q}^-, u^-)$ be the values of the gradient and displacement on the same edge considered as part of the other element. Then we introduce for the interior edges $e \in \mathcal{E}_h^o$:

$$\begin{aligned} \{\{\mathbf{q}\}\} &= (\mathbf{q}^+ + \mathbf{q}^-)/2 & \{\{u\}\} &= (u^+ + u^-)/2 \\ [\![\mathbf{q} \cdot \mathbf{n}]\!] &= \mathbf{q}^+ \cdot \mathbf{n}^+ + \mathbf{q}^- \cdot \mathbf{n}^- & [\![u]\!] &= u^+\mathbf{n}^+ + u^-\mathbf{n}^- \end{aligned} \tag{2.3}$$

Note how the average of a vector is a vector and the average of a scalar is a scalar but the jumps are defined for the magnitudes times the normal so for the gradient it becomes a scalar and for the displacement it is a vector. We still need to extend this definition to the boundary edges and we do that as follows. For $e \in \mathcal{E}_h^\partial$:

$$\begin{aligned} \{\{\mathbf{q}\}\} &= \mathbf{q} & \{\{u\}\} &= u \\ [\![\mathbf{q} \cdot \mathbf{n}]\!] &= \mathbf{q} \cdot \mathbf{n} & [\![u]\!] &= u \cdot \mathbf{n} \end{aligned} \tag{2.4}$$

[1]Might not be equal to Ω if the domain is curved and $\mathcal{T}_h$ only considers linear elements, for instance.

[2]Note that $\mu_d(\cdot)$ indicates the d dimension Lebesgue measure of the set $\cdot$.

Finally let's introduce the notation used for the contractions or L^2 dot products of functions over elements and boundaries. Say $\mathbf{u}, \mathbf{v} \in [L^2(D)]^d$ and $u, v \in L^2(D)$, then we denote the scalar products in the interior and over the edges as in (2.5):

$$\begin{aligned} (\mathbf{u}, \mathbf{v})|_D &= \int_D \mathbf{u} \cdot \mathbf{v}\, dV \quad \langle \mathbf{u}, \mathbf{v} \rangle|_{\partial D} = \int_{\partial D} \mathbf{u} \cdot \mathbf{v}\, dS \\ (u, v)|_D &= \int_D u \cdot v\, dV \quad \langle u, v \rangle|_{\partial D} = \int_{\partial D} u \cdot v\, dS \end{aligned} \tag{2.5}$$

2.3.2 Key idea

One can really think of the Hybridizable Discontinuous Galerkin method formulation from a quite abstract point of view in which we split the global problem into a number of local ones in each element. Some extra variables are created such that the problems can actually be separated and split up. Afterwards we solve a global problem that matches all boundary interface terms. So let K be an element in $\mathcal{T}_h$. Let also λ be any given function on ∂K. Then we consider the following problem:

$$\begin{aligned} \mathbf{q}^\lambda - \nabla u^\lambda &= 0, && \text{in } K \\ \nabla \cdot \mathbf{q}^\lambda &= k^2 u^\lambda, && \text{in } K \\ u^\lambda &= \lambda, && \text{on } \partial K \end{aligned} \tag{2.6}$$

It can be observed that, in fact, if

$$\lambda = u|_{\partial K} \tag{2.7}$$

we are solving our original problem (2.2), that is $(\mathbf{q}^\lambda, u^\lambda) = (\mathbf{q}, u)$. Hence our main objective is to find λ that satisfies (2.7). In order to do that, we will define the so called global problem which will require λ to satisfy

$$\begin{aligned} \lambda &= g_D, && \text{on } \partial\Omega_D, \\ \mathbf{q}^\lambda \cdot \mathbf{n} &= g_N, && \text{on } \partial\Omega_N, \\ (\mathbf{q}^\lambda)^+ \cdot \mathbf{n}^+ + (\mathbf{q}^\lambda)^- \cdot \mathbf{n}^- &= 0, && \text{on } e, \forall e \in \mathcal{E}_h^o. \end{aligned} \tag{2.8}$$

So, in the end, we find λ solution for the global problem (2.8) using the fact that all local solutions come from (2.6) which is actually the key idea of the HDG method.

2.3.3 Aproximation spaces

First let $\mathcal{P}^k(\Omega)$ be the set of polynomials of degree at most k over a domain Ω[3]. The discontinuous finite element spaces that we are about to use are described in (2.9). Note that we need three spaces: one for the scalar displacement, another for the gradient which is a vector, and yet another scalar space need be defined on the edges of the discretization.

$$\begin{aligned} W_h^k &= \{\omega \in L^2(\Omega) : \omega|_K \in W^k(K), \forall K \in \mathcal{T}_h\}, \\ \mathbf{V}_h^k &= \{\mathbf{p} \in [L^2(\Omega)]^d : \mathbf{p}|_K \in \mathbf{V}^k(K), \forall K \in \mathcal{T}_h\}, \\ M_h^k &= \{\mu \in L^2(\mathcal{E}_h) : \mu|_e \in M^k(e), \forall e \in \mathcal{E}_h\}. \end{aligned} \tag{2.9}$$

Recall that $L^2(\Omega)$ is the space of square integrable functions over Ω. Let's consider $\tilde{g}_D$ the L^2 projection of the Dirichlet boundary condition into the polynomial space described above for the boundaries and then set $M_h^k(g_D) = \{\mu \in M_h^k : \mu|_{\Gamma_D} = \tilde{g}_D\}$.

2.3.4 Space discretization

The first thing in which we are interested is turning the system of equations in (2.2) into a weak formulation. In order to do that, we contract the equations for the discretized version of the variables by given test functions in the corresponding (Dirichlet homogeneous)[4] spaces. Using the notation previously introduced, that is shown in (2.10).

$$\begin{aligned} (\mathbf{q}_h, \mathbf{v})_K + (\nabla u_h, \mathbf{v})_K &= 0, \quad \forall \mathbf{v} \in [\mathcal{P}^k(K)]^d \\ (\nabla \cdot \mathbf{q}_h, w)_K &= (k^2 u_h, w)_K, \quad \forall w \in \mathcal{P}^k(K) \end{aligned} \tag{2.10}$$

[3]Boldfacing $\mathcal{P}$ would create a vector set of polynomials of degree at most k over the same Ω.

[4]See any FE textbook in order to see further explanation on that. But basically we know that the Dirichlet boundary conditions show up on the definition of the discretization space and we obtain the variational formulation by computing the first order variations for a solution which is the addition of the discretized variables plus the test functions, which we thus require to be homogeneous Dirichlet if we want this new solution to still be a consistent solution.

Now we carry out an integration by parts of the volume terms containing the nabla operator in order to obtain (2.11). So, in the end, we are interested in looking for an approximation $(\mathbf{q}_h, u_h) \in \mathbf{V}_h^k \times W_h^k$ such that, for all element K of the triangulation $\mathcal{T}_h$ equation (2.11) holds.

$$\begin{aligned} (\mathbf{q}_h, \mathbf{v})_K - (u_h, \nabla \cdot \mathbf{v})_K + \langle \hat{u}_h, \mathbf{v} \cdot \mathbf{n} \rangle_{\partial K} = 0, \quad & \forall \mathbf{v} \in [\mathcal{P}^k(K)]^d \\ -(\mathbf{q}_h, \nabla w)_K + \langle \hat{q}_h \cdot \mathbf{n}, w \rangle_{\partial K} = (k^2 u, w)_K, \quad & \forall w \in \mathcal{P}^k(K) \end{aligned} \tag{2.11}$$

Note how, in the integration by parts, the degrees of freedom at the boundaries have been replaced by the numerical traces or fluxes since the variables themselves are not well defined there. After that, using the HDG approach, we need to specify $\hat{\mathbf{q}}_h$ in terms of $\mathbf{q}_h, u_h, \hat{u}_h$.

$$\hat{\mathbf{q}}_h = \mathbf{q}_h + \tau(u_h - \hat{u}_h), \text{ on } \partial K \tag{2.12}$$

The stabilization parameter τ is taken to be a positive constant of order unity. Further analysis on how to choose τ can be found in [34] for instance and the optimal election of it will give place to the superconvergence treated in a later section whereas a naive choice will just recover the classic DG scheme.

Similarly we still need to obtain an expression for $\hat{u}_h$ in order to be able to fully separate the local and global problems. That is, we want to be able to solve locally for every element and then globally over the nodes on the boundaries thus we will obtain the numerical trace for u as follows.

$$\hat{u}_h = \begin{cases} \tilde{g}_D, & \text{on } \mathcal{E}_h \cap \Gamma_D \\ \lambda_h, & \text{on } \mathcal{E}_h \backslash (\Gamma_D \cap \mathcal{E}_h) \end{cases} \tag{2.13}$$

where $\lambda_h \in M_h^k(0)$ is a new variable that will allow the assembling of the local problem into the global. Finally by adding up all contributions of (2.11) over the elements on the triangulation $\mathcal{T}_h$ and also enforcing the continuity of the normal component of

the numerical flux, we obtain the global system of equations shown in (2.14).

$$\begin{aligned}
&(\mathbf{q}_h, \mathbf{v})_{\mathcal{T}_h} - (u_h, \nabla \cdot \mathbf{v})_{\mathcal{T}_h} + \langle \lambda_h, \mathbf{v} \cdot \mathbf{n} \rangle_{\partial \mathcal{T}_h \setminus \mathcal{E}_h^\partial} = -\langle g_D, \mathbf{v} \cdot \mathbf{n} \rangle_{\Gamma_D}, && \forall \mathbf{v} \in \mathbf{V}_h^k, \\
&-(\mathbf{q}_h, \nabla w)_{\mathcal{T}_h} + \langle \hat{q}_h \cdot \mathbf{n}, w \rangle_{\partial \mathcal{T}_h} = (k^2 u_h, w)_{\mathcal{T}_h}, && \forall w \in W_h^k, \\
&\langle [\![\hat{\mathbf{q}}_h \cdot \mathbf{n}]\!], \mu \rangle_{\mathcal{E}_h} = \langle g_N, \mu \rangle_{\Gamma_N}, && \forall \mu \in M_h^k(0).
\end{aligned} \tag{2.14}$$

If we now plug the expression for the numerical fluxes in (2.12) and (2.13) into the previous equations (2.14) and we redo some integration by parts for convenience in the notation, we obtain the final system to solve as shown in (2.15).

$$\begin{aligned}
&(\mathbf{q}_h, \mathbf{v})_{\mathcal{T}_h} - (u_h, \nabla \cdot \mathbf{v})_{\mathcal{T}_h} + \langle \lambda_h, \mathbf{v} \cdot \mathbf{n} \rangle_{\partial \mathcal{T}_h} = -\langle g_D, \mathbf{v} \cdot \mathbf{n} \rangle_{\Gamma_D}, && \forall \mathbf{v} \in \mathbf{V}_h^k, \\
&(\nabla \cdot \mathbf{q}_h, w)_{\mathcal{T}_h} + \langle \tau u_h, w \rangle_{\partial \mathcal{T}_h} - \langle \tau \lambda_h, w \rangle_{\partial \mathcal{T}_h} = (k^2 u_h, w)_{\mathcal{T}_h}, && \forall w \in W_h^k, \\
&\langle \mathbf{q}_h \cdot \mathbf{n}, \mu \rangle_{\mathcal{E}_h} + \langle \tau u_h, \mu \rangle_{\mathcal{E}_h} - \langle \tau \lambda_h, \mu \rangle_{\mathcal{E}_h} = \langle g_N, \mu \rangle_{\Gamma_N}, && \forall \mu \in M_h^k(0).
\end{aligned} \tag{2.15}$$

2.3.5 Implementation and system solution

The system of equations in (2.15) can actually be rewritten in terms of some bilinear forms as follows. Find $(\mathbf{q}_h, u_h, \lambda_h) \in \mathbf{V}_h^k \times W_h^k \times M_h^k(0)$ such that

$$\begin{aligned}
&a(\mathbf{q}_h, \mathbf{v}) - b(u_h, \mathbf{v}) + c(\lambda_h, \mathbf{v}) = r(\mathbf{v}), \\
&b(w, \mathbf{q}_h) + d(u_h, w) + e(\lambda_h, w) = f(w), \\
&c(\mu, \mathbf{q}_h) + g(\mu, u_h) + h(\mu, \lambda_h) = s(\mu).
\end{aligned} \tag{2.16}$$

holds for all $(\mathbf{v}, w, \mu) \in \mathbf{V}_h^k \times W_h^k \times M_h^k(0)$. Where the bilinear functions are given by

$$\begin{aligned}
&a(\mathbf{q}, \mathbf{v}) = (\mathbf{q}, \mathbf{v})_{\mathcal{T}_h}, && b(u, \mathbf{v}) = (u, \nabla \cdot \mathbf{v})_{\mathcal{T}_h}, \\
&c(\lambda, \mathbf{v}) = \langle \lambda, \mathbf{v} \cdot \mathbf{n} \rangle_{\partial \mathcal{T}_h}, && d(u, w) = \langle \tau u, w \rangle_{\partial \mathcal{T}_h}, \\
&e(\lambda, w) = -\langle \tau \lambda, w \rangle_{\partial \mathcal{T}_h}, && f(w) = (k^2 u, w)_{\mathcal{T}_h}, \\
&g(\mu, u) = \langle \tau u, \mu \rangle_{\mathcal{E}_h}, && h(\mu, \lambda) = \langle \tau \lambda, \mu \rangle_{\mathcal{E}_h}, \\
&r(\mathbf{v}) = -\langle g_D, \mathbf{v} \cdot \mathbf{n} \rangle_{\Gamma_D}, && s(\mu) = \langle g_N, \mu \rangle_{\Gamma_N}.
\end{aligned} \tag{2.17}$$

for all $(\mathbf{q}, u, \lambda) \in \mathbf{V}_h^k \times W_h^k \times M_h^k$.

The discretization of the system of equations given in (2.16) gives rise to a matrix

equation summarized in (2.18).

$$\begin{bmatrix} \mathbb{A} & -\mathbb{B}^T & \mathbb{C}^T \\ \mathbb{B} & \mathbb{D} & \mathbb{E} \\ \mathbb{C} & \mathbb{G} & \mathbb{H} \end{bmatrix} \begin{bmatrix} \mathbf{Q} \\ \mathbf{U} \\ \mathbf{\Lambda} \end{bmatrix} = \begin{bmatrix} \mathbf{R} \\ \mathbf{F} \\ \mathbf{S} \end{bmatrix} \tag{2.18}$$

Note that $\mathbf{Q}$ represents the variables associated with the $\mathbf{q}_h$ degrees of freedom, $\mathbf{U}$ those related to u_h and similarly $\mathbf{\Lambda}$ those of $\hat{u}_h$. As it has already been reasoned, the particular great advantage of using HDG versus other Discontinuous Galerkin approaches will show up right here. After the consideration of the numerical traces as degrees of freedom instead of setting them beforehand as classic DG would do, it turns out that all the equations regarding the variables $\mathbf{q}_h$ and u_h depend **only** on local variables and hence the system can be solved separately for each element leading to a very efficient method.

This fact can be mathematically understood as follows. $\mathbb{A}, \mathbb{B}, \mathbb{D}$ will be not only sparse but also block diagonal matrices and thus will be all zeros except from some centered positions corresponding to the $\mathbf{Q}$ and $\mathbf{U}$ in the corresponding element. With all, we can carry out a rearrangement (2.19) of the variables and order them in an elementwise fashion.

$$\begin{bmatrix} (\mathbf{Q}_1, U_1) & \cdots & (\mathbf{Q}_N, U_N) \end{bmatrix}^T = \mathbb{P} \begin{bmatrix} \mathbf{Q} \\ \mathbf{U} \end{bmatrix} \tag{2.19}$$

being $\mathbb{P}$ a permutation matrix that just rearranges the rows of the local subsystem of equations. Let's assume our system matrix has already been rearranged and keep the same previous notation for convenience.

After these manipulations we can now proceed to solve the system of equations in (2.18) efficiently. In the end, we obtain the following two relations (2.20) and (2.21) for the transformed system.

$$\begin{bmatrix} \mathbf{Q} \\ \mathbf{U} \end{bmatrix} = \begin{bmatrix} \mathbb{A} & -\mathbb{B}^T \\ \mathbb{B} & \mathbb{D} \end{bmatrix}^{-1} \left(\begin{bmatrix} \mathbf{R} \\ \mathbf{F} \end{bmatrix} - \begin{bmatrix} \mathbf{C}^T \\ \mathbf{E} \end{bmatrix} \mathbf{\Lambda} \right), \tag{2.20}$$

and

$$\mathbb{C}\mathbf{Q} + \mathbb{G}\mathbf{U} + \mathbb{H}\mathbf{\Lambda} = \mathbf{S}. \tag{2.21}$$

The procedure will therefore be based on solving first equation (2.20) locally for each element of the discretization[5] and once $\mathbf{Q}$ and $\mathbf{U}$ has been obtained in terms of $\mathbf{\Lambda}$, plug the expressions in equation (2.21) and solve globally for $\mathbf{\Lambda}$. Once more, note how the global system is solved only over the elements on the edges and never within the inside of each element. Finally we obtain the system for $\mathbf{\Lambda}$ as shown in equation (2.22) by plugging in (2.20) into (2.21).

$$\mathbb{K}\mathbf{\Lambda} = \mathbf{T} \tag{2.22}$$

where both $\mathbb{K}$ and $\mathbf{T}$ are given by

$$\mathbb{K} = -\begin{bmatrix} \mathbb{C} & \mathbb{G} \end{bmatrix} \begin{bmatrix} \mathbb{A} & -\mathbb{B}^T \\ \mathbb{B} & \mathbb{D} \end{bmatrix}^{-1} \begin{bmatrix} \mathbf{C}^T \\ \mathbf{E} \end{bmatrix} + \mathbb{H} \tag{2.23}$$

and

$$\mathbf{T} = \mathbf{S} - \begin{bmatrix} \mathbb{C} & \mathbb{G} \end{bmatrix} \begin{bmatrix} \mathbb{A} & -\mathbb{B}^T \\ \mathbb{B} & \mathbb{D} \end{bmatrix}^{-1} \begin{bmatrix} \mathbf{R} \\ \mathbf{F} \end{bmatrix} \tag{2.24}$$

So we proceed to solve globally for $\mathbf{\Lambda}$ and then we go into (2.20) and obtain both $\mathbf{Q}$ and $\mathbf{U}$ doing all the local solves. Table 2.1 summarizes the algorithm to implement the previously described method.

Table 2.1: HDG algorith for the Helmholtz Equation

1.-	Compute all matrices for the bilinear forms ($\mathbb{A}, \mathbb{B}, \mathbb{D}$ just locally),
2.-	Invert elemental matrices $\mathbb{A}, \mathbb{B}, \mathbb{D}$ and assemble them into a global matrix,
3.-	Generate the global matrix $\mathbb{K}$ and vector $\mathbf{T}$,
4.-	Solve the global system for $\mathbf{\Lambda}$ using (2.22),
5.-	Solve locally for $\mathbf{Q}$ and $\mathbf{U}$ using (2.20).

[5]Parallelization has not been taken into account in this thesis and nor has it been implemented here but this part is totally parallelizable.

2.4 1st order absorbing boundary conditions

One very important point in the final implementation of the code are the boundary conditions. Most of the problems that are to be considered will consist on a point or planar[6] source wave which will propagate[7] throughout a material, and then will leave the domain. In order to avoid reflections, the boundary conditions at the outflow boundaries need be analyzed carefully.

It is clear then that the term *absorbing* boundary conditions actually comes from its meaning for the time dependent wave equation. However and since we solve the wave propagation problem using the steady state Helmholtz equation, absorbing boundary condition still need to be considered. The use of absorbing boundary conditions has been widely studied (see [11], for instance). Nguyen et al. derive them for the time dependent wave equation in [40]. Another approaches to treat the absorbing boundary conditions are based on the construction of Perfectly Matched Layers (aka PMLs), a brief and clear explanation of them can be found in [22].

So we consider solving the steady wave equation modeled through the Helmholtz equation as described in the previous section. Say Γ_{abs} defines the boundary of the domain where the wave escapes from the domain and therefore we want to avoid reflections. Then we are going to consider the following boundary condition

$$\frac{d\tilde{u}}{dt} + \tilde{\mathbf{q}} \cdot \mathbf{n} = 0, \text{ on } \Gamma_{abs} \tag{2.25}$$

Once more, our u is not time dependent but equation (2.25) refers to the second order time dependent wave equation. Recall from section 1.2.1 that $\tilde{u}(x,t) = u(x)e^{i\omega t}$ and from there we derived the Helmholtz equation. With all, for our particular case we can write,

$$\left[(i\omega)u + \mathbf{q} \cdot \mathbf{n} = 0\right] e^{i\omega t}, \text{ on } \Gamma_{abs} \tag{2.26}$$

Furthermore, we want the above condition to be satisfied for the scattered field

[6] These will be to simulate very faraway point sources

[7] Actually not. The Helmholtz equation simulates only the steady state but since its derivation here comes from the wave equation all the examples will still refer to the time dependent wave equation, although analyzed steadily.

actually, and not for the total field. That is, we do not want the boundaries to absorb all the waves but only the ones which would be reflected. Say we write the scattered field as $u^s = u - u^i$ where u is the total field and $u^i = e^{i\mathbf{k}\cdot\mathbf{x}}$ represents the incident field. Similarly, consider the decomposition of the flux as $\mathbf{q}^s = \mathbf{q} - \mathbf{q}^i$.

$$i\omega u^s + \mathbf{q}\cdot\mathbf{n} = 0 \Leftrightarrow i\omega u + \mathbf{q}\cdot\mathbf{n} = i\omega u^i + \mathbf{q}^i\cdot\mathbf{n} \tag{2.27}$$

Now consider left and right hand side boundaries, where the normal takes either $(1,0)$ or $(-1,0)$ and we will derive the particular expression for planar boundaries (which are most of them). Then the absorbing boundary condition can actually be written as

$$\begin{cases} i\omega u + \mathbf{k}\nabla u = 0, & \text{for the left hand side} \\ i\omega u - \mathbf{k}\nabla u = 2ike^{i\mathbf{k}\cdot\mathbf{x}}, & \text{for the right hand side} \end{cases} \tag{2.28}$$

and note how this includes the total absorbing boundary condition for the right side, say, and the source term for the left side, if that is the setting we seek.

2.5 Superconvergence

One of the most appealing properties of the Hybridizable Discontinuous Galerkin Method versus other DG approaches shows up when analyzing the convergence rate of the computed solutions. It is shown in [20] that

$$||u - u_h||_{L^2(\mathcal{T}_h)} \leq C|u|_{H^{k+1}(\mathcal{T}_h)}h^{k+1/2} \tag{2.29}$$

holds for the standard DG method. In practice, most examples lead to an optimal convergence of $k+1$ but cases where the $1/2$ is obtained have been found and hence the above convergence estimate is tight. Placing further constraints on the mesh it can be proved that the convergence can be pushed up to $k+1$. The HDG formulation gives, however, a better rate of convergence after a local postprocessing.

Say u_h^* is the displacement solution after the postprocessing treatment that we are about to describe, then it has been proved in [9] for some HDG cases that the

convergence rate estimate introduced in [3] still applies. That is,

$$||u - u_h^*||_{L^2(\mathcal{T}_h)} \leq C|u|_{H^{k+2}(\mathcal{T}_h)} h^{k+2} \tag{2.30}$$

Note however that the postprocessing is only enabled by the fact that both u and $\mathbf{q}$ converge as $k+1$ as shown in (2.31). Given the optimal convergence of u and $\mathbf{q}$ it is possible to devise a local efficient procedure to obtain the $k+2$ displacement solution convergence.

$$\begin{aligned} ||u - u_h||_{L^2(\mathcal{T}_h)} &\leq C|u|_{H^{k+2}(\mathcal{T}_h)} h^{k+1} \\ ||\mathbf{q} - \mathbf{q}_h||_{L^2(\mathcal{T}_h)} &\leq C|\mathbf{q}|_{H^{k+2}(\mathcal{T}_h)} h^{k+1} \end{aligned} \tag{2.31}$$

2.5.1 Local Postprocessing

A local postprocessing procedure is carried out element by element and therefore is highly parallelizable as well as cheap and efficient to do. The key point is to be able to exploit the optimal convergence of $\mathbf{q}_h$ which together with the superconvergence properties of u_h will lead to the sought convergence rate for the displacement. It must yet be said that this superconvergence property is not only achieved by the HDG method but also by other FEM approaches such as the hybridized RT and the hybridized BDM methods as shown in [5, 6].

Let's first begin by seeking the postprocessed total flux. We are interested in finding $\mathbf{q}_h^* \in [\mathcal{P}_k(K)]^d + \mathbf{x}\mathcal{P}_{k+1}(K)$ for all K in the triangulation $\mathcal{T}_h$ such that,

$$\begin{aligned} \langle(\mathbf{q}_h^* - \hat{\mathbf{q}}_h)\cdot\mathbf{n}, \mu\rangle_e &= 0, \quad \forall \mu \in \mathcal{P}_k(e), \forall e \in \partial K \\ (\mathbf{q}_h^* - \mathbf{q}_h, \mathbf{v})_K &= 0, \qquad \forall \mathbf{v} \in [\mathcal{P}_{k-1}(K)]^d \text{ if } k > 1 \end{aligned} \tag{2.32}$$

where once more $\hat{\mathbf{q}}_h = \mathbf{q}_h - \tau(u - \hat{u}_h)$. According to equation (2.32) we see that $\mathbf{q}_h^*$ is actually the Thomas-Raviart projection of $\mathbf{q}$. Furthermore, $\mathbf{q}_h^*$ is in $H(div, \Omega)$[8] thanks to the fact of having a unique value for the normal component of the numerical trace. It is also shown in [5] that the rate of convergence of both $\mathbf{q}_h^*$ and $\mathbf{q}$ are the

[8]This means that its normal component is continuous across the interelement boundaries.

same. Note the difference between the two: $\mathbf{q}_h$ is discontinuous over $\mathcal{T}_h$ whereas $\mathbf{q}_h^*$ is an $H(div,\Omega)-$conforming function.

Now we still need to compute u_h^* and that can be done solving the system defined in (2.33). We need to find $(u_h^*, \mathbf{q}_h^*, \lambda_h^*) \in \mathcal{P}_{k+1}(K) \times [\mathcal{P}_{k+1}(K)]^d \times [\mathcal{P}_{k+1}(e)]^{d+1}$ on every $K \in \mathcal{T}_h$ and every $e \in \mathcal{E}_h$ such that equation (2.33) is satisfied for all $(v, \mathbf{w}, \mu) \in \mathcal{P}_{k+1}(K) \times [\mathcal{P}_{k+1}(K)]^d \times [\mathcal{P}_{k+1}(e)]^{d+1}$.

$$\begin{aligned}
(\nabla \mathbf{q}_h^*, \mathbf{w})_K - (u_h^*, \nabla \cdot \mathbf{w})_K + \langle \lambda_h^*, \mathbf{w} \cdot \mathbf{n} \rangle_{\partial K} &= 0, \\
-(\mathbf{q}_h^*, \nabla v)_K + \langle \hat{\mathbf{q}}_h^* \cdot \mathbf{n}, v \rangle_{\partial K} &= (\nabla \cdot \mathbf{q}_h^*, v)_K, \\
\langle \hat{\mathbf{q}}_h^* \cdot \mathbf{n}, \mu \rangle_{\partial K} &= \langle \mathbf{q}_h^* \cdot \mathbf{n}, \mu \rangle_{\partial K}, \\
(u_h^*, 1)_K &= (u_h, 1)_K.
\end{aligned} \tag{2.33}$$

In fact, the system in equation (2.33) is the Galerkin discretization of the following diffusion Neumann problem,

$$\begin{aligned}
-\nabla^2 u &= \nabla \cdot \mathbf{q}_h^*, \qquad \text{in } K \\
-\nabla u \cdot \mathbf{n} &= \mathbf{q}_h^* \cdot \mathbf{n}. \qquad \text{on } \partial K \\
(u, 1)_K &= (u_h, 1)_K.
\end{aligned} \tag{2.34}$$

for every single triangulation element K and where $\mathbf{q}_h^*$ is the postprocessed total flux from (2.32).This procedure allows us to evaluate u and obtain a convergence rate of $k+2$.

2.5.2 A Numerical Example

In order to be able to numerically check the above derivations, a convergence test is carried out for a simple problem. Let's consider a rectangular domain with a given uniform material (say $\mathbf{k} = (1, 0)$). Furthermore we will consider a planar wave propagating from the left to the right so Neumann boundary conditions are assumed in both upper and lower boundaries. However for the left and right side boundaries equation (2.28) has been considered for absorbing boundaries.

For this particular setting we know the solution to the Helmholtz equation which

is actually given by

$$u(x) = \cos(x) + i\sin(x) \quad x \in [0, 10] \tag{2.35}$$

Say the rectangular domain is of size 10×1 and since air (propagation speed equal 1) has been considered the frequency will be $\omega = kc = 1$ and 10 periods will fit within the domain. Figure 2-2 shows the exact solution for the defined problem.

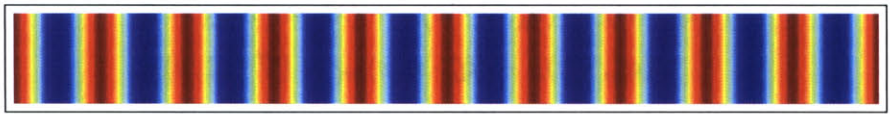

Figure 2-2: Real part of the solution for the Superconvergence test setting

Figure 2-3 shows the convergence rate for a polynomial order of approximation of $3, 4, 5$ and different mesh sizes. The corresponding data are collected in tables 2.2,2.3,2.4. Note how u^* superconverges always (i.e. $k + 2$) with one order higher than either u and $\mathbf{q}$ which converge with $k + 1$.

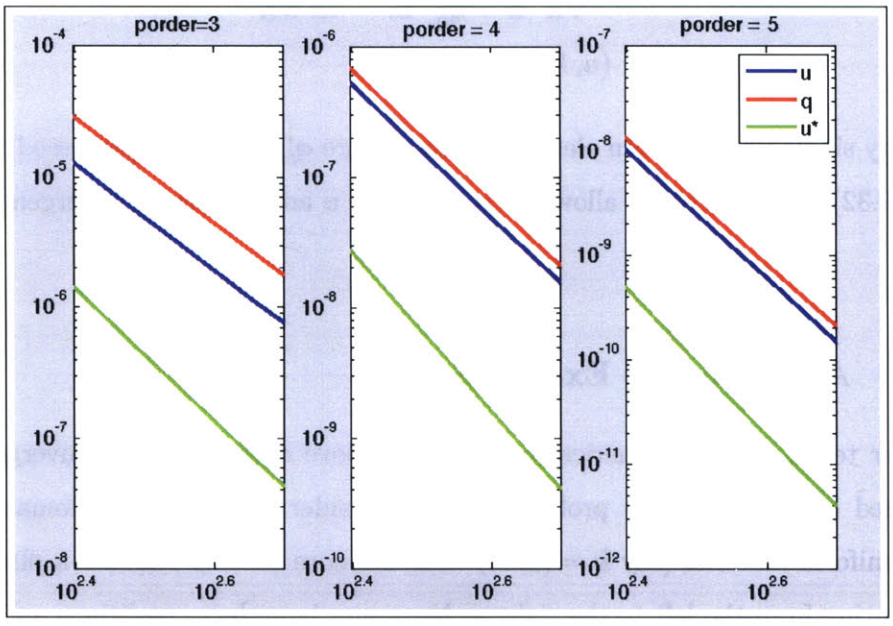

Figure 2-3: Convergence rate plots for the planar wave propagation

Table 2.2: Convergence rate for the planar wave propagation example for a polynomial order of approximation of 3 and different sizes of the mesh

Degree	Mesh	$\|\|u-u_h\|\|_{L^2}$		$\|\|\mathbf{q}-\mathbf{q}_h\|\|_{L^2}$		$\|\|u-u_h^*\|\|_{L^2}$	
p	n_e	*lerror*	order	*error*	order	*error*	order
3	250	1.30e-5	-	2.95e-5	-	1.44e-6	-
	300	6.15e-6	4.023	1.41e-5	4.054	5.69e-7	5.081
	350	3.26e-6	4.022	7.52e-6	4.058	2.60e-7	5.079
	400	1.88e-6	4.019	4.37e-6	4.061	1.32e-7	5.077
	450	1.16e-6	4.015	2.70e-6	4.063	7.28e-8	5.075
	500	7.55e-7	4.011	1.76e-6	4.064	4.27e-8	5.072

Table 2.3: Convergence rate for the planar wave propagation example for a polynomial order of approximation of 4 and different sizes of the mesh

Degree	Mesh	$\|\|u-u_h\|\|_{L^2}$		$\|\|\mathbf{q}-\mathbf{q}_h\|\|_{L^2}$		$\|\|u-u_h^*\|\|_{L^2}$	
p	n_e	*lerror*	order	*error*	order	*error*	order
4	250	5.32e-7	-	6.78e-7	-	2.72e-8	-
	300	2.10e-7	5.003	2.71e-7	5.016	9.04e-9	6.049
	350	9.57e-8	5.007	1.25e-7	5.015	3.56e-9	6.049
	400	4.83e-8	5.009	6.42e-8	5.014	1.58e-9	6.048
	450	2.65e-8	5.001	3.55e-8	5.014	7.79e-10	6.047
	500	1.55e-8	5.002	2.09e-8	5.014	4.12e-10	6.046

Table 2.4: Convergence rate for the planar wave propagation example for a polynomial order of approximation of 5 and different sizes of the mesh

Degree	Mesh	$\|\|u-u_h\|\|_{L^2}$		$\|\|\mathbf{q}-\mathbf{q}_h\|\|_{L^2}$		$\|\|u-u_h^*\|\|_{L^2}$	
p	n_e	*lerror*	order	*error*	order	*error*	order
5	250	1.05e-8	-	1.35e-8	-	4.92e-10	-
	300	3.45e-9	6.007	4.53e-09	5.999	1.36e-10	7.022
	350	1.34e-9	6.011	1.80e-9	5.998	4.63e-11	7.022
	400	5.93e-10	6.014	8.09e-10	5.997	1.82e-11	7.019
	450	2.89e-10	6.017	3.99e-10	5.999	8.04e-12	7.000
	500	1.51e-10	6.018	2.12e-10	5.996	4.04e-12	6.992

Chapter 3

Material design optimization

As it has already been introduced in the first chapter, most of the metamaterials found in the literature have been derived using physical intuition. In fact, without such intuition there would have been no way of finding any kind of configuration attaining properties such as the bandgap, for instance. However, once physicists have introduced this field and have found many applications as well as some solutions, there is now some room for mathematicians and, more precisely, optimizers to find optimal solutions. This need arises since some of the structures or patterns that metamaterials show are highly non intuitive and very difficult to predict unless optimization techniques lead you there.

Within this community some optimal structures have already been designed although most of them can only locally be applied to a particular problem. Thus, there is the incessant need of finding some general procedure that can be applied to different problems. The main objective of this chapter is therefore to classify the different optimization problems that can be formulated in this context and provide suitable techniques for them. Nevertheless, it must be said from the very beginning that most of the optimization problems that arise in this field are non-convex and highly complex. For this reason, global optima will seldom be found and thus local optima that are 'good enough' will be the desired solutions.

3.1 Types of optimization problems

The two main types of problems that will be found within this context can be classified as Optimal Control problems and Eigenvalue Optimization problems. The former are the most general and can be easily reformulated for a wide range of applications. The latter arise basically when bandgap maximization is sought or, in general, when we want to either maximize or minimize an objective function that depends on the eigenvalues of a system. Although we are interested in solving both types of problems, for the sake of this thesis efforts will focus on the Optimal Control problems.

3.1.1 Optimal Control problems

Say we want to find some metamaterial satisfying a given wave propagation property. We send some incoming wave to a given domain and we desire to design the material properties of a given region in the domain such that the outgoing wave is as close as possible to some beforehand known and set wave. Figure 3-1 shows a possible schematic setting for an optimal control problem in metamaterial design. We send some incoming wave from the left boundary and seek to know the optimal design in region D such that the wave pattern u in region R is as close as possible to a known value $\bar{u}$.

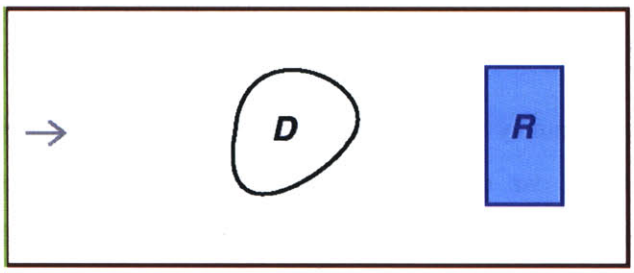

Figure 3-1: General setting for an optimal control problem

The mathematical formulation for this problem has already been introduced in equation (1.4). Hence, what we want to minimize is a given norm (usually the L^2 norm) of the difference between the numerically computed output and the desired

one in region R. The constraints are given by the governing equation, a volume constraint and the already relaxed boxed constraints for the design variables, which will be further discussed in the next section.

Thus we write equation (3.1). Note that now $\boldsymbol{\alpha} \in \mathbb{R}^n$ is the vector of design variables, assumed to be constant over each element. Q is a positive definite matrix.

$$\begin{aligned} \min_{\boldsymbol{\alpha},u} \quad & (u-\bar{u})^T Q(u-\bar{u}) \\ \text{s.t.} \quad & \mathcal{F}(\boldsymbol{\alpha},u) = f \\ & \alpha_{min} \leq \boldsymbol{\alpha} \leq \alpha_{max} \\ & \mathbf{1}^T\boldsymbol{\alpha} \leq \xi \end{aligned} \tag{3.1}$$

If the volume constraint is incorporated to the objective function and what we seek are solutions with smallest integrated value of α, the optimization formulation can also be written as in (3.2),

$$\begin{aligned} \min_{\boldsymbol{\alpha},u} \quad & (u-\bar{u})^T Q(u-\bar{u}) + \varphi(\mathbf{1}^T\boldsymbol{\alpha}) \\ \text{s.t.} \quad & \mathcal{F}(\boldsymbol{\alpha},u) = f \\ & \alpha_{min} \leq \boldsymbol{\alpha} \leq \alpha_{max} \end{aligned} \tag{3.2}$$

where φ represents the dual variable. In order to carry out the optimization, classic descent algorithms will be used. Particular issues about the implementation as well as further considerations about the optimization algorithms used will be taken into account in section 3.3.

Some of the problems that can fit in this class are, for example, the frequency filters, where we seek to minimize the difference between a given input, which is a superposition of a set of linear waves, and the desired output, which is the superposition of only the waves with the frequency outside the range to be filtered. Furthermore, the cloaking problem fits also in this class since we want to design the properties on the cloaking region such that the wave at the right hand side of the domain equals the incoming wave from the left side of the domain, no matter what you put inside the cloak. In addition to these applications, we can also consider the superlensing device,

where we look for a metamaterial distributed in a rectangular (thus flat) region and that is able to reproduce a given source in one side into the other side. These are just some applications but many others could also be considered within this framework.

3.1.2 Eigenvalue optimization problems

The different types of problems that are addressed in this thesis are governed by PDEs. Such PDEs can also give rise to eigenproblems. Thus, we will sometimes be interested in maximizing the heat transfer over a certain material, which can be interpreted as maximizing the largest eigenvalue of a discretized heat transfer equation. Similarly, we might also be interested in maximizing the photonic bandgap for a certain material. Such photonic bandgap can be characterized by a combination of eigenvalues of the discretization of Maxwell's Equations, see [27, 28] for instance.

Furthermore, some eigenvalue optimization problems can be stated in terms of Semidefinite Programming (SDP-optimization) techniques, which offer fantastic and efficient algorithms. In a general setting, assume we are dealing with a problem of the form of (3.3) for some full-rank matrices A and M. Let's also say that we want to maximize the largest eigenvalue.

$$A(\boldsymbol{\alpha})\mathbf{u} = \lambda M\mathbf{u} \tag{3.3}$$

We can write the largest eigenvalue maximization problem as follows:

$$\begin{aligned} \min_{\boldsymbol{\alpha}} \quad & -\mu \\ \text{s.t.} \quad & A(\boldsymbol{\alpha}) - \mu M \succeq 0 \end{aligned} \tag{3.4}$$

where the objective function has been multiplied by -1 in order to obtain a minimization problem. Moreover, problem (3.4) turns up to be convex and can be easily written as an SDP formulation. Thus it can be solved efficiently and accurately.

Note that if $A - \mu M \succeq 0$ for $\mu \geq \lambda_{max}$ then it is also positive definite for all other eigenvalues. Similarly, the minimization of the smallest eigenvalue can also be written in such a way and the problem we end up having is also convex and written

in terms of an SDP formulation. Note however that the maximization of the smallest eigenvalue or the minimization of the largest one is not really convex and cannot be written as above. There are some other eigenvalue expressions that can be written in this way and thus the corresponding optimization problems can all be efficiently solved, see [43, 49].

The introduction of approximate subspaces also allow for the maximization or minimization of essentially any eigenvalue within the range. The price we are paying is the approximation, which sometimes is not as accurate as desired, as well as the loss of convexity.

3.2 Dealing with the box constraints

In our original problem we are interested in solutions with either one material or the other and thus we look for $\alpha \in \{\alpha_{min}, \alpha_{max}\}$ instead. However, we know that solving binary or discrete optimization problems is $NP-$hard[1] and this is something we really want to avoid.

One might think that the relaxation just introduced will lead to very different solutions and this is, in general, true. Nevertheless, some good solutions can sometimes be obtained without enforcing the binary constraint and allowing the variables to be in the continuous range $\alpha_{min} < \alpha < \alpha_{max}$. It was already claimed by Lord Rayleigh in 1887 [48] that 1d photonic crystals would always tend to maximize contrast within the design variables and therefore a $\{0, 1\}$ solution would always lead to better results than any possible $(0, 1)$ solution. This remarkable property has been experimentally and numerically observed in 2d and 3d applications although there is yet no proof for that. Results in [27, 28] have been found using optimization with the above relaxed box constraints and therefore its computational cost has been dramatically reduced from the one obtained when using classic discrete optimization algorithms such as,

[1] $NP-$hard means that any algorithm developed for its numerical computation has a cost greater than any polynomial order. It is thought that actually $NP \neq P$ and therefore no polynomial order algorithm can be found to solve such problems. However such claim is one of the Clay Mathematics Institute seven millennium questions that is yet not answered, i.e. proved.

for instance, branch and bound, which basically needs to compare solutions in all possible points (note that combinations of solutions $\{0,1\}^n$ grows exponentially as n is increased).

Unfortunately, this great property is not observed in other problems, even if optimized using the same techniques and formulations. Despite the bad news, we still want to avoid using discrete constraints for the optimization problems since they will be, at times, of large size and exponential computational costs are just impractical. Some naive solution would be just to solve the problem with the relaxed version of the constraints and after one or a few iterations project the solution into the discrete values and carry on the optimization. Clearly here the convergence is not guaranteed and further considerations will need to be taken into account for the solution of general problems.

3.3 Optimal control problem for $1d$ bandgap optimization

Consider a rectangular domain in 2d and a wave propagating from left to right. The leftmost boundary will be therefore considered as the inflow boundary and a planar wave will be sent into the domain. Here, we will use the first order absorbing boundary conditions described in the previous chapter. The rightmost side of the rectangular domain will be the outflow boundary and thus the corresponding absorbing boundary conditions will also be required. Finally, both top and bottom boundaries will be considered to be pure homogeneous Neumann since this will give the 1d character to the problem, even though the simulations are run in 2d.

It is well known (see, for instance, [19]) that the dispersion relation (ω vs. k)[2] corresponding to a certain homogeneous material is given by a line, essentially $\omega = \pm ck$, where c is the propagation speed of sound/light[3] for such homogeneous media.

[2]From now on, ω denotes the frequency of a certain linear wave and k the wavenumber or wavevector depending on the dimensionality of the problem.

[3]Depending whether we deal with acoustic waves or electromagnetic

However we can assume that there is some periodicity a in this same homogenous material (see figure 3-2-top) and then, if we reproduce the same straight lines starting from different period distances we obtain a dispersion relation as the one shown in figure 3-3-left.

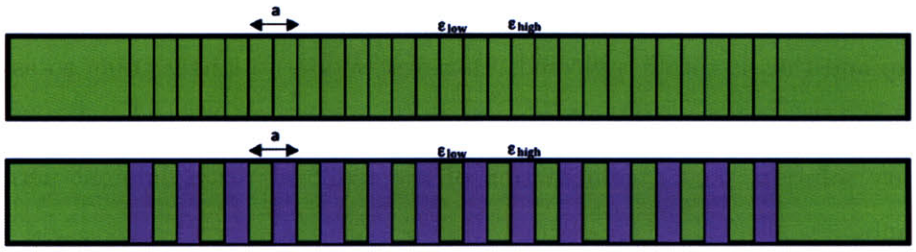

Figure 3-2: Top: a periodicity considered in a rectangular homogeneous pattern. Bottom: a periodic material pattern with a permittivity contrast of 13 to 1

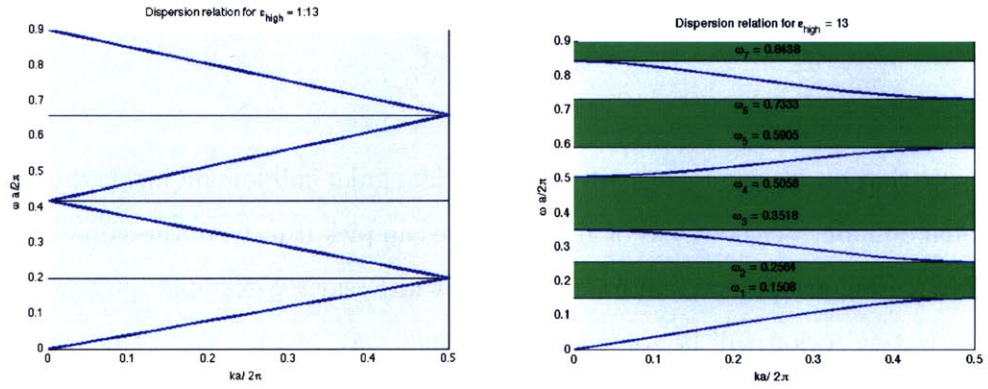

Figure 3-3: Dispersion relation for the Left: homogeneous pattern. Right: periodic material with a permittivity contrast of 13 to 1

Besides, if we now change a little bit the material properties in some of the parts of the domain keeping the periodicity we will open a gap. That is, if we increase the contrast between the permittivities conforming the periodic material we will keep on increasing the magnitude of some ranges of frequency for which there is no corresponding k. Such ranges are called bandgaps . Physically, this means that for a frequency in the bandgap, there will be no propagation[4] throughout the correspond-

[4]It can actually be shown that there will be an exponentially decaying solution propagating throughout the material.

ing periodic material. Figure 3-2-bottom shows a certain periodic material with a permittivity contrast of $\varepsilon_{high}/\varepsilon_{low} = 13$ and the corresponding dispersion relation is given in figure 3-3-right.

We are now ready to formulate the optimal control problem that we are interested in solving. Say that we want to find a setting for which a certain frequency is inside the gap and thus is totally reflected. However we are no longer going to assume an infinite domain and thus the solution might not be a periodic material. We look for a binary solution. i.e. a combination of two materials with different permittivity constants.

Using the notation in section 3.1.1 we want to solve the optimization problem written in (3.5).

$$\begin{aligned} \min_{\boldsymbol{\varepsilon},\mathbf{u}} \quad & \mathbf{u}^T M \mathbf{u} \\ \text{s.t.} \quad & A(\boldsymbol{\varepsilon})\mathbf{u} = \mathbf{f} \\ & \varepsilon_{low} \leq \boldsymbol{\varepsilon} \leq \varepsilon_{high} \end{aligned} \tag{3.5}$$

Note that our design region will be some rectangular subdomain inside the computational domain. Without loss of generality we can pick it to be of the same height as the big rectangle and a certain fraction of the width, say for example $1/5$[5]. Moreover, the objective region will be some other rectangle, say, of the exact same size as the design region, but in the righthandside of the design region. Figure 3-4 shows the domains that are involved in the setting up of this problem.

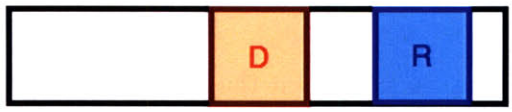

Figure 3-4: Domain definition for the bandgap problem

The equation $A(\boldsymbol{\varepsilon})\mathbf{u} = \mathbf{f}$ in (3.5) corresponds to the discretization of the Helmholtz equation solved using the HDG method discribed in the previous chapter. The matrix

[5]We are actually interested in minimizing this width, since narrower design regions will lead to more compact designs.

M in the objective function is actually the mass matrix defined by the shape functions considered in the HDG Finite Element Method with the particularity that it also restricts the the solution u to the objective region R in figure 3-4. That is, $||\mathbf{u}||_2 = (\mathbf{u}, \mathbf{u})$ would be given by the same exact expression but with the entire mass matrix M. Here the mass matrix is only nonzero for the corresponding terms of the solution $\mathbf{u}$ in R.

3.3.1 Adjoint based optimization

The adjoint method is a very common approach for solving optimization problems involving PDEs. The adjoint method is a computationally very effective way of computing the gradients of a certain function g of a solution $\mathbf{u}$ and some design variables $\boldsymbol{\alpha}$. Some further and deeper analysis on these methods can be found in [2, 12, 21], for instance. All in all, whenever we have, as above, an optimization problem with the objective function being some $g(\mathbf{u}, \boldsymbol{\alpha})$ and subject to $\mathbf{u}$ being the solution of a discretized PDE (the helmholtz equation in our case), the adjoint method provides us with $dg/d\boldsymbol{\alpha}$ with a constant cost, i.e. independently of the size of the design variables. In a general setting we are to solve the following problem:

$$\begin{aligned} \min_{\boldsymbol{\alpha},\mathbf{u}} \quad & g(\mathbf{u}, \boldsymbol{\alpha}) \\ \text{s.t.} \quad & h(\mathbf{u}, \boldsymbol{\alpha}) = 0 \end{aligned} \tag{3.6}$$

After the dualization of the constraint, the objective function can be written as $G(\mathbf{u}, \boldsymbol{\alpha}, \boldsymbol{\phi}) = g(\mathbf{u}, \boldsymbol{\alpha}) + \boldsymbol{\phi}^T h(\mathbf{u}, \boldsymbol{\alpha})$ and thus, if we compute the sensitivities with respect to the design variables $\boldsymbol{\alpha}$, we obtain:

$$\begin{aligned} \frac{\partial}{\partial \boldsymbol{\alpha}} G(\mathbf{u}, \boldsymbol{\alpha}, \boldsymbol{\phi}) = 0 \quad &\Leftrightarrow \frac{\partial g}{\partial \boldsymbol{\alpha}} + \frac{\partial g}{\partial \mathbf{u}} \frac{\partial u}{\partial \boldsymbol{\alpha}} + \boldsymbol{\phi}^T \frac{\partial h}{\partial \mathbf{u}} \frac{\partial \mathbf{u}}{\partial \boldsymbol{\alpha}} + \boldsymbol{\phi}^T \frac{\partial h}{\partial \boldsymbol{\alpha}} = 0 \\ &\Leftrightarrow \frac{\partial g}{\partial \boldsymbol{\alpha}} + \boldsymbol{\phi}^T \frac{\partial h}{\partial \boldsymbol{\alpha}} + \left(\frac{\partial g}{\partial \mathbf{u}} + \boldsymbol{\phi}^T \frac{\partial h}{\partial \mathbf{u}} \right) \frac{\partial \mathbf{u}}{\partial \boldsymbol{\alpha}} = 0 \end{aligned} \tag{3.7}$$

We choose the adjoint $\boldsymbol{\phi}$ in such a way that the parenthesized expression in the last line of equation (3.7) vanishes. In this way, we are able to compute the sensitivities

with respect to the design variables without having to compute the sensitivities of $\mathbf{u}$ with respect to the same design variables, which are computationally very expensive. Thus, we need to pick $\boldsymbol{\phi}$ satisfying (3.8), which will be called the Adjoint Equation.

$$\frac{\partial g}{\partial \mathbf{u}} + \boldsymbol{\phi}^T \frac{\partial h}{\partial \mathbf{u}} = 0 \tag{3.8}$$

And once the adjoint has been computed we can compute the sensitivities just as shown in (3.9).

$$\frac{\partial}{\partial \boldsymbol{\alpha}} G(\mathbf{u}, \boldsymbol{\alpha}, \boldsymbol{\phi}) = \frac{\partial g}{\partial \boldsymbol{\alpha}} + \boldsymbol{\phi}^T \frac{\partial h}{\partial \boldsymbol{\alpha}} \tag{3.9}$$

Note that whenever $h(\mathbf{u}, \boldsymbol{\alpha}) = 0$ represents the discretization of a PDE, the adjoint equation (3.9) can be interpreted in terms of a new PDE for the adjoint variable $\boldsymbol{\phi}$. Since the Helmholtz equation is self-adjoint, the governing PDE for $\boldsymbol{\phi}$ will then be exactly the same Helmholtz equation with the addition of a source term associated with the objective function. The boundary conditions required will also be derived in a straightforward manner when solving (3.8). The particular derivation of all the above described equations for the bandgap problem can be found in section 4.2.1.

The adjoint approach works well for calculating sensitivities when we deal with continuous variables. In our case, we are interested in discrete variables and we rely on projecting the solution onto the extrema. It turns up that for the problem considered here, this approach works reasonably well. However, it must be said that some other approaches could be considered, either based on forcing the gradients to always give binary solutions (topological gradient methods) or performing a robust optimization and modify the optima a posteriori in order to make it binary.

Chapter 4

Numerical results

This chapter summarizes the set of results obtained for some particular problems formulated using all the derivations in previous chapters. It is split up in two sections. The first section corresponds to the results on simulations whereas the second section presents the optimization results.

4.1 Simulation of linear wave phenomena

This section shows the results of simulating some well known linear wave phenomena using the implemented algorithms. First of all, results on the $1d$ photonic bangap problem already introduced in previous chapters are provided. We can secondly find an extension from such example called the frequency filter. There, we will look for patterns that, not only do they filter out some frequencies by containing them in the gap but they also let some other frequencies of interest go through without any reflection. The understanding and simulation of this particular problem will be of interest since the maximization of bandgap ranges will be of interest together with the fact of not affecting the frequencies outside the gap (total transmission for them), which will be further analyzed in the optimization of these problems within the next section. After these two $1d$ examples some 2d cloaking simulations are also presented.

4.1.1 Bandgap in $1d$

The problem setting for the $1d$ photonic bandgap problem has already been provided in section 3.3. In this subsection we are interested in providing accurate and high order simulations of the Helmholtz equation in a rectangular domain. A normalized period a has been chosen as well as a permittivity contrast of 1 to 13. For the infinitely periodic setting the dispersion relation is the one shown in figure 4-1.

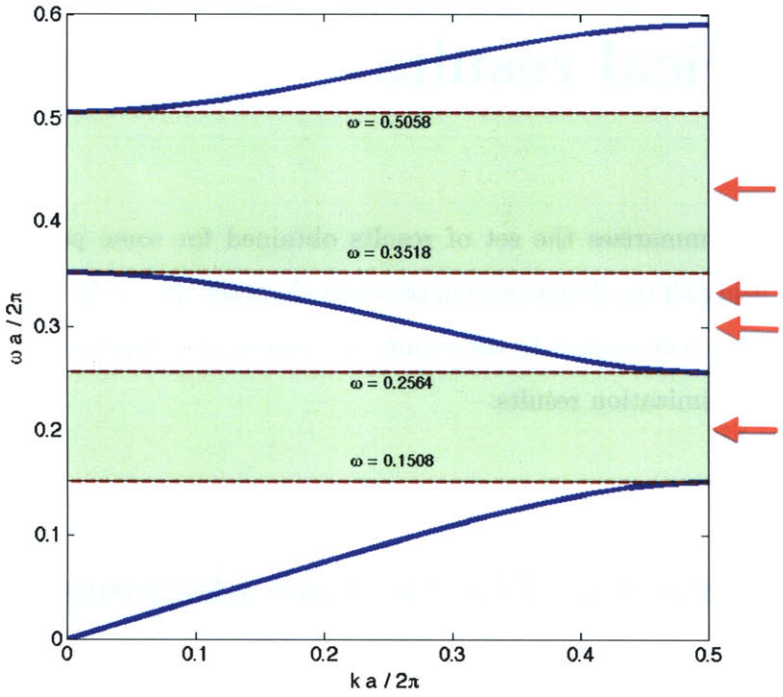

Figure 4-1: Dispersion relation for the infinitely-periodic pattern used for the simulations. Axis are normalized for the period a, i.e. vertical axis corresponds to $\omega a/2\pi$ and the horizontal to $ka/2\pi$. The four analyzed frequencies are shown through the righthandside arrows.

We use the HDG code and perform simulations for four different frequencies. Firstly let's consider a certain frequency ω_1 inside the lowest gap as shown in figure 4-2. Note that the dispersion relation in figure 4-1 corresponds to an assumed infinite-many amount of periods which is clearly something we are not going to have in our case. Thus, we might expect slightly different results, meaning basically two issues: firstly, any frequency close enough to the gap boundary, either from above or below,

is going to perform a transition from being transmitted to being totally reflected (this would not happen in the infinite case); moreover, the frequencies outside the gap are not going to be totally transmitted since the lack of infinite periodicity is going to result in some fractional reflection and some transmission.

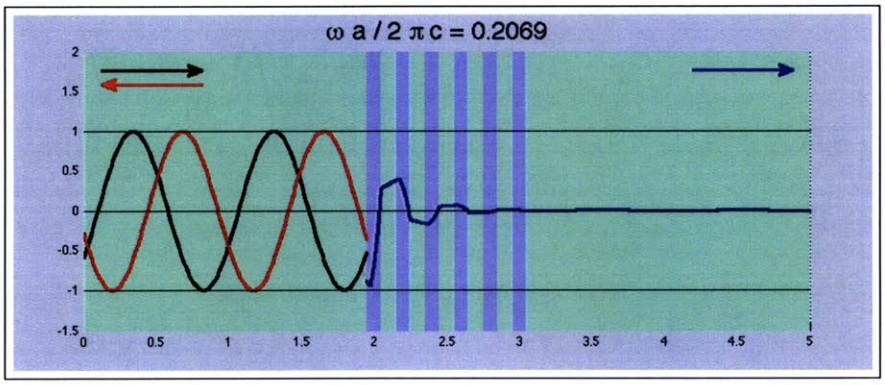

Figure 4-2: Propagation pattern through a 6 periods pattern with normalized period a for the frequency $\omega_1 a/2\pi = 0.2069$. In black the incoming wave to the left, in red the reflected wave and in blue the propagated wave.

After that, we consider a frequency ω_2 outside the gap, carefully chosen so that it results in total transmission and no reflection. However, as explained and due to the finiteness of the domain, we do not expect such behavior and thus a third frequency ω_3 slightly tuned up is also simulated resulting in some transmission and some reflection.

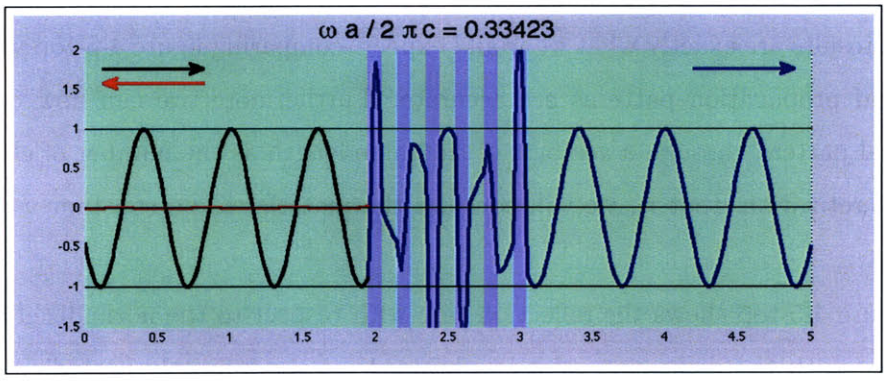

Figure 4-3: Propagation pattern through a 6 periods pattern with normalized period a for the frequency $\omega_2 a/2\pi = 0.33423$. In black the incoming wave to the left, in red the reflected wave and in blue the propagated wave.

Finally, if we keep on tuning up the frequency into ω_4 we will enter again the bandgap. All these cases are shown in figures 4-3 and 4-4.

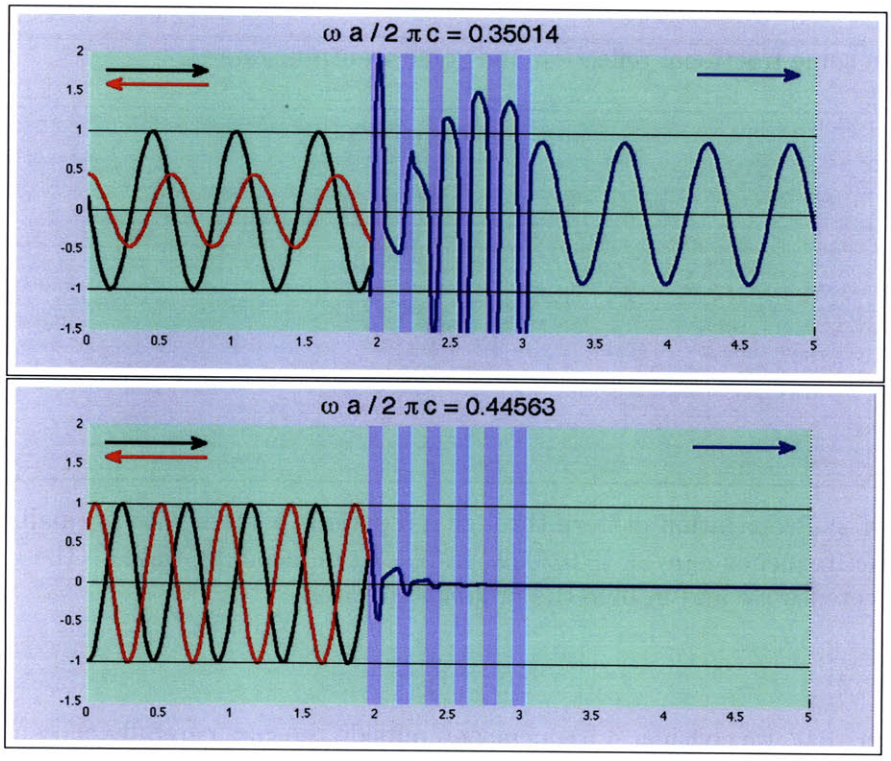

Figure 4-4: Propagation pattern through a 6 periods pattern with normalized period a for the frequencies $\omega_3 a/2\pi = 0.35014$ and $\omega_4 a/2\pi = 0.44563$. In black the incoming wave to the left, in red the reflected wave and in blue the propagated wave.

All results are exactly what we would expect (comparing figure 4-5-top with figure 4-1) and propagation patterns are accurate. Furthermore, we can now define any material pattern through a vector $\boldsymbol{\epsilon}$ of the same length as the number of elements in the discretization, that is, we will consider the material to be constant within each element.

Figure 4-5-top shows the reflection rate with respect to the normalized omega to compare with the dispersion relation obtained for the infinitely periodic equivalent pattern. Note how we still obtain bandgaps for the exact same ranges of frequencies and also note the interesting behavior of the wave pattern for any frequency outside the bandgap. In fact, this will have consequences when we carry out the optimization.

It is not only that the reflection function is highly non convex/non concave (with respect with either the frequency or the the material contrast). It is also interesting to see how robust the plot is for a frequency in the gap: that is, if a frequency is quite in the middle of the gap, any small enough (but quite large) perturbation of either the frequency or the pattern itself will still be in the gap. However, that can clearly not be said for a totally transmitted frequency, which only happens for point frequencies and thus any tiny perturbation would produce terrible effects. Similarly figure 4-5-bottom shows the same reflection rate for a given normalized frequency of $\omega = 0.4775$ when changing the contrast of the two materials from 1 (homogeneous) to 25.

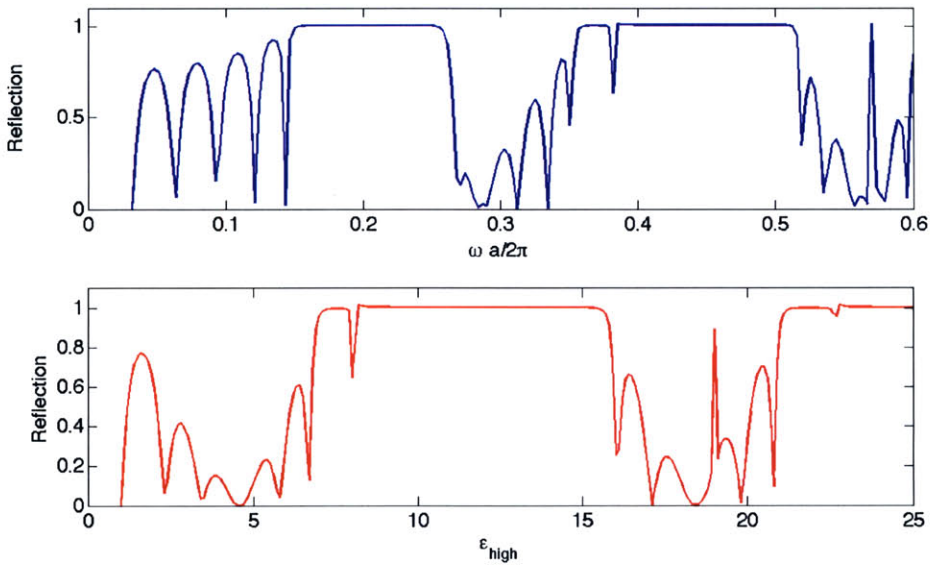

Figure 4-5: Top: Reflection rate versus the normalized frequency for 6 periodic pattern used in figures 4-2 to 4-4 and for a permittivity contrast of 1 to 13. Bottom: Reflection rate versus the permittivity of the second material ε_{high} for a frequency of $\omega = 0.4775$.

4.1.2 Frequency filter in $1d$

A quite straightforward extension of the example introduced in the previous section is to consider a linear combination of linear waves with different frequencies and

amplitudes such that, for a certain periodic pattern, one of them is totally transmitted at the same time as the other one is totally reflected. If we actually consider ω_2 and ω_4 and build up a linear combination of them, say just the addition of them two, we are going to obtain the simulation of desired frequency filter. Figure 4-6 shows this result. Note how a linear wave signal can be easily split into its linear components.

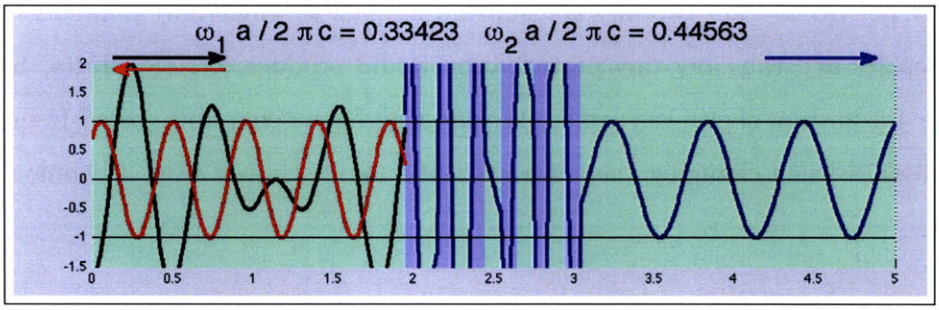

Figure 4-6: Propagation pattern through a 6 periods pattern with normalized period a for a linear wave resulting of the addition of the waves of $\omega_2 a/2\pi = 0.33423$ and $\omega_4 a/2\pi = 0.44563$. In black the incoming superposition of the two waves going to the left, in red the totally reflected wave for ω_4 and in blue the totally propagated wave ω_2.

This application will be particularly interesting from the point of view of optimization. In fact, due to the behavior of either the reflection or the transmission with respect to tuning either the contrast of the permittivities or the frequency itself, it will not be possible to create a range of frequencies for which the material behaves as totally homogeneous (100% transmission). It will be interesting, though, to maximize the bandgap keeping a certain frequency transmitted. A number of particular and different problems arise and can be formulated related to the simulations we are now able to run.

4.1.3 Cloaking in $2d$

The design of a cloaking device has been desired and analyzed since ancient times. It has always been in the wish list of most communities and it seems that nowadays we are really getting closer and closer to achieve such goal. In fact, it was already firstly introduced by Pendry et al. in Science [45] through a singular change of variables

that will actually be analyzed more carefully within this section. A lot of research groups have recently been working on the design of cloaking devices in both $2d$ and $3d$ with some interesting results achieved.

Several efforts can be found in the literature for the Helmholtz equation cloaking through the changes of variables proposed by Pendry in [23, 30] for instance. Some other more general articles about cloaking are [14, 17, 29], amongst others. At this point we are just interested in being able to adapt the code for the simulation of this problem and thus we will try to reproduce how the approach presented in [45] works. All in all, we seek to design a material in the annular blue region in figure 4-7 such that for any incoming wave the object in the inner circular region is hidden, meaning that the wave propagation pattern outside the cloaking device (blue region) is unchanged by the presence of the inner circle and the cloaking device.

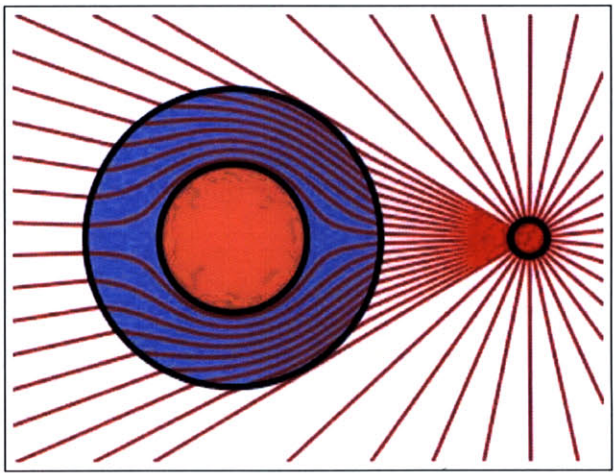

Figure 4-7: From Pendry et al. in [45]. Cloaking working scheme.

The change of variables proposed by Pendry et al. in [45] turns up to be singular at the interior boundary of the cloaking region since it is mapping a full rectangular subset of $\mathbb{R}^2$ into the same rectangle but taking out a circle inside. The point corresponding to the center of the circle will thus be mapped into the whole $\mathbb{S}_1$ boundary in the image space. In fact, the change of variables there introduced can be reduced

in the $2d$ case to the following change on the permittivity.

$$\varepsilon_r = \frac{r-a}{r} \quad \varepsilon_\theta = \frac{r}{r-a} \tag{4.1}$$

where a is the inner radius of the cloaking ring. Note how the new permittivity is not isotropic and has different values in the radial and circumferential directions. The HDG formulation has been adapted accordingly to deal with a tensorial ε or propagation speed c. Analytically, what this change of variables is doing is just pushing out the wave streamlines (orthogonal to the contours of the waves shown in figure 4-8) smoothly around the cloaked object.

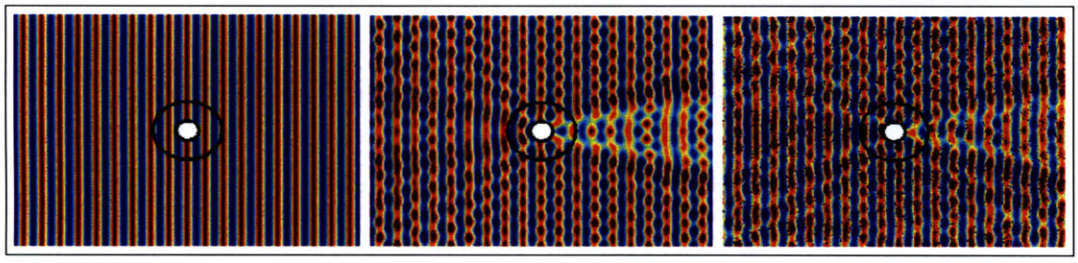

Figure 4-8: Cloaking propagation pattern. Left: incident wave sent (without any object). Center: Propagation pattern when no metamaterial is considered in the cloaking ring. Right: Solution pattern using the $a = 0.5$ approach of Pendry et al. change of variables.

However and since this approach can not be reproduced numerically due to the singularity (check how ε_θ blows up for the points approaching the inner radius) some approximation needed to be considered for the simulations at this point. Say we pick $a = 0.5$ times the inner radius, instead of directly the inner radius. For this particular case the angular permittivity does not blow up close to the inner radius, it just grows a little bit. Clearly the results will not provide full cloaking of the device but, for sure, we should observe some modification of the wave pattern towards the cloaking case.

Figures 4-8 and 4-9 show the propagation pattern with and without the approximate cloaking ring as well as the difference between the solutions and the desired totally invisible wave pattern. Note how the solution gets closer to the one without

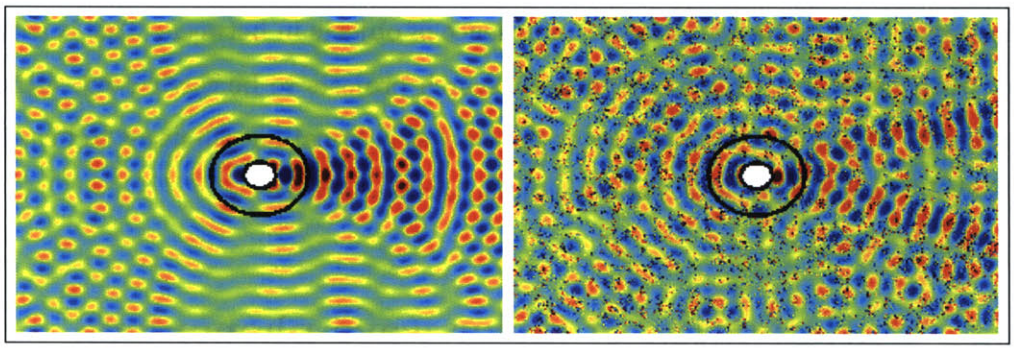

Figure 4-9: Difference between the propagation patterns and the no-object solution. Left: when including the circular object. Right: when cloaking it with the $a = 0.5$ approximation.

any object in the region when we consider the described approximation of the singular change of variables proposed in [45]. This actually remarks the need of designing some metamaterial allowing not only for anisotropy but also for a binary combination of materials such that the cloaking effect can be realized. In the end we need to formulate an optimization problem corresponding to the sketch shown in figure 4-10 using the optimal control formulations introduced in the previous chapter.

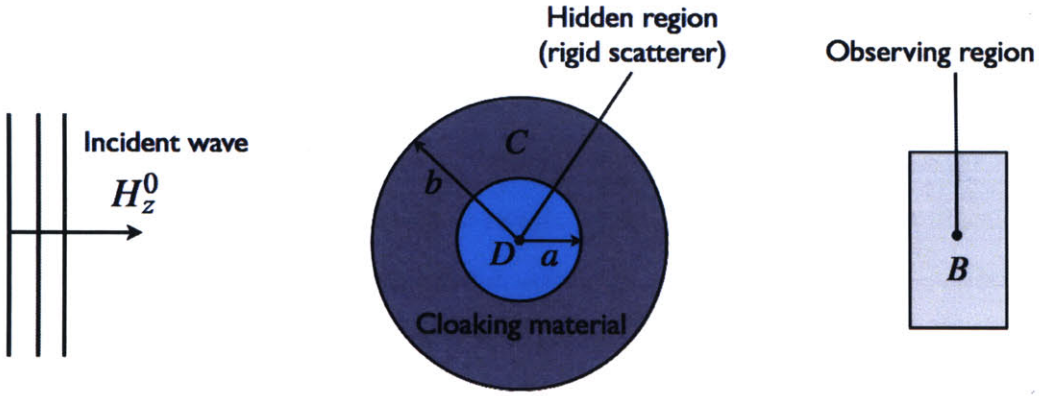

Figure 4-10: Cloaking setting for the optimal control formulation of the problem.

Figure 4-10 summarizes the problem setting for the optimization process using the optimal control techniques. Incident waves are sent from the left and the observing region B is considered to be on the right. Inside this observing region is where we seek to minimize the distance between the wave solution for a certain material distribution

in region C and the known solution in absence of objects in between. This is actually one of the most interesting near future research projects to be carried out, although the binary optimization techniques or the Robust Fabrication still needs to be pushed a little bit in order to really attain manufacturable devices.

4.2 Optimization of linear wave phenomena

Once we have validated our capability for simulation of linear wave phenomena, we can move on and start to perform some optimization on the already described problems. We will focus on the application of the adjoint method optimization on the $1d$ bandgap problem.

4.2.1 Bandgap in $1d$

Section 3.3.1 described how to use the adjoint method in a general context. For our particular case of the $1d$ bandgap problem recall that we have to solve the optimization problem in (4.2). Let's call $g(\mathbf{u}, \boldsymbol{\varepsilon}) = \int_R \mathbf{u}^T \mathbf{u}\, dV$, the L^2 norm of the solution over the objective region domain R.

$$\begin{aligned} \min_{\boldsymbol{\varepsilon},\mathbf{u}} \quad & g(\mathbf{u}, \boldsymbol{\varepsilon}) \\ \text{s.t.} \quad & A(\boldsymbol{\varepsilon})\mathbf{u} = f \\ & \varepsilon_{low} \leq \boldsymbol{\varepsilon} \leq \varepsilon_{high} \end{aligned} \tag{4.2}$$

Moreover and as explained in section 3.3.1, we can now use duality techniques to push the PDE based constraint into the objective function and thus define $G(\mathbf{u}, \boldsymbol{\varepsilon}, \boldsymbol{\phi})$ as in equation (4.3). Recall that for the case we are dealing with, $A(\boldsymbol{\varepsilon})\mathbf{u} = \mathbf{f}$ is the discretization of Helmholtz equation which can be written as $-\nabla \cdot (c^2 \nabla \mathbf{u}) - \omega^2 \mathbf{u}$, just as in equation (2.1) and using the fact that $\omega = kc$.

Our aim will be to find a $\boldsymbol{\phi}$ such that the objective function is as simple as possible while still imposing the same PDE constraint. That is, we push the constraint into the objective function through a dual variable $\boldsymbol{\phi}$ and rearrange the terms on the new

objective function.

$$
\begin{aligned}
G(\mathbf{u},\boldsymbol{\varepsilon},\boldsymbol{\phi}) &= g(\mathbf{u},\boldsymbol{\varepsilon}) + \int_R \boldsymbol{\phi}^T (A(\boldsymbol{\varepsilon})\mathbf{u} - \mathbf{f})\, dV = \\
&= \int_R \mathbf{u}^T \mathbf{u}\, dV + \int_R \boldsymbol{\phi}^T (\nabla \cdot (c^2 \nabla \mathbf{u}) - \omega^2 \mathbf{u})\, dV = \\
&= \int_R \mathbf{u}^T \mathbf{u}\, dV + \int_R (-\nabla \boldsymbol{\phi}^T c^2 \nabla \mathbf{u} - \omega^2 \mathbf{u})\, dV + \int_{\partial R} \boldsymbol{\phi}^T c^2 \nabla \mathbf{u} \cdot \vec{n}\, dS = \\
&= \int_R \mathbf{u}^T \mathbf{u} - \nabla \boldsymbol{\phi}^T c^2 \nabla \mathbf{u} - \omega^2 \mathbf{u}\, dV + \int_{\partial R} \boldsymbol{\phi}^T c^2 \nabla \mathbf{u} \cdot \vec{n}\, dS
\end{aligned}
\tag{4.3}
$$

The third line results from performing an integration by parts on the dual term[1]. In (4.4) we show the derivations of the weak formulation of the Adjoint Problem, which will let us derive the sensitivities of G.

$$
\begin{aligned}
\frac{\partial g}{\partial \mathbf{u}} + \boldsymbol{\phi}^T \frac{\partial h}{\partial \mathbf{u}} = 0 \Leftrightarrow \\
\int_R 2\mathbf{u}\, dV + \frac{\partial}{\partial \mathbf{u}} \int_R \boldsymbol{\phi}^T (\nabla \cdot (c \nabla \mathbf{u}) - \omega^2 \mathbf{u})\, dV = 0 \Leftrightarrow \\
\int_R 2\mathbf{u}\, dV + \frac{\partial}{\partial \mathbf{u}} \int_R (-\nabla \boldsymbol{\phi}^T c \nabla \mathbf{u} - \boldsymbol{\phi}^T \omega^2 \mathbf{u})\, dV + \frac{\partial}{\partial u} \int_{\partial R} \boldsymbol{\phi}^T c \nabla \mathbf{u} \cdot \vec{n}\, dS = 0 \Leftrightarrow \\
\int_R 2\mathbf{u}\, dV + \frac{\partial}{\partial \mathbf{u}} \int_R (\nabla (c \nabla \boldsymbol{\phi}^T)\mathbf{u} - \boldsymbol{\phi}^T \omega^2 \mathbf{u})\, dV + \frac{\partial}{\partial u} \int_{\partial R} -\mathbf{u} c \nabla \boldsymbol{\phi} \cdot \vec{n}\, dS = 0 \Leftrightarrow \\
\int_R 2\mathbf{u}\, dV + \int_R (\nabla (c \nabla \boldsymbol{\phi}^T) - \boldsymbol{\phi}^T \omega^2)\, dV = 0 \Leftrightarrow
\end{aligned}
\tag{4.4}
$$

Between the third and fourth line we have chosen $\boldsymbol{\phi} = 0$ on the left and right boundaries in order for the boundary term to vanish everywhere. Similarly between

[1]Boldfacing indicates vectors related to the discretization, $\vec{\cdot}$ notation is related to vectors in the sense of x and y components. Although c represents a function of the material distribution, in the end it will become a vector $\mathbf{c}$ of constant values in certain discretized regions.

the fourth and fifth line we have chosen $\nabla\boldsymbol{\phi}\cdot\vec{n}=0$ on the top and bottom boundaries for the boundary integral to vanish everywhere too. All in all, will obtain the adjoint equation for this problem just through the same technique as in (3.8) which gives the result in the adjoint problem (4.5) if we state it in a strong manner.

$$\begin{cases} 2\mathbf{u}+\nabla\cdot(c^2\nabla\boldsymbol{\phi})-\omega^2\boldsymbol{\phi}=0 & \text{in D} \\ \nabla\boldsymbol{\phi}\cdot\vec{n}=0 & \text{on top and bottom} \\ \boldsymbol{\phi}=0 & \text{on left and right} \end{cases} \tag{4.5}$$

where D is the subdomain where we want to match solutions. Clearly, the equation is defined over the whole domain but we only consider u to be non-zero in the region where we want to match the target and computed waves. It is now clear why this method is called the Adjoint Method. The governing PDE for $\boldsymbol{\phi}$ is exactly the adjoint of the initial governing PDE. Furthermore, in this case since the equation is selfadjoint, we actually obtain the same equation except from the source terms matching up the objective function. Note how the boundary conditions chosen for $\boldsymbol{\phi}$ are actually analogous to the ones of $\mathbf{u}$ since we want all the boundary terms in the last equation of (4.3) to vanish. That is, since $\nabla\mathbf{u}\cdot\vec{n}=0$ in the top and bottom boundaries of the domain, we will need $\boldsymbol{\phi}=0$ at the other two boundaries (where $\mathbf{u}$ is also zero), i.e. left and right, and reversely for the other two boundaries.

For the particular problem we are dealing with, there is no direct dependence of g on the design variables $\boldsymbol{\varepsilon}$ and thus, equation (3.9) can be written as in (4.6). This will give us the sensitivities in which we are interested once we already know what the adjoint variable $\boldsymbol{\phi}$ is.

$$\frac{\partial}{\partial\boldsymbol{\varepsilon}}G(\mathbf{u},\boldsymbol{\varepsilon})=-\int_R\nabla\boldsymbol{\phi}\nabla\mathbf{u}\,dV \tag{4.6}$$

After all that, we now want to solve the problem in (4.2) which will be done just by a classic Descent Method (a Steepest Descent will be a good enough approach for now) but using the gradient information provided by the Adjoint Method proposed and derived. Moreover, we still need to take care of the box constraints and that will

be done when determining the stepsize. We will make sure that all our solutions are always feasible just by picking the largest stepsize possible always imposing all ε to be in our valid range. This method works pretty well but still is not the best possible approach since our solutions are not guaranteed to provide binary values. In fact, the method might, however, get stuck due to the box constraints (imagine it wants to move further a pixel that already has the maximum value). If that happens we can either change the initial guess or, more cleverly, let it do some iterations and at a certain point just clip de solution by our valid range and continue iterating.

Table 4.1 summarizes the algorithm used for solving the optimal control optimization problems using the just described technique based on Adjoint Methods. Results for this implementation will be provided just below.

Table 4.1: Algorithm for the $1d$ Bandgap Problem Optimization using the Adjoint Method formulation

	Algorithm 4.1
1-	Give some initial guess $\boldsymbol{\varepsilon}^0$ and provide the corresponding $\mathbf{u}^0$
2-	Compute the adjoint solving (4.5)
3-	Compute the sensitivities $\nabla_{\boldsymbol{\varepsilon}} G(\mathbf{u}, \boldsymbol{\varepsilon})$ through (4.6)
4-	Define some stepsize α and find the new $\boldsymbol{\varepsilon}^1$. Make sure it is feasible i.e. pick α s.t. $\varepsilon_{low} \leq \varepsilon_i \leq \varepsilon_{high}, \forall \varepsilon_i$
5-	Compute the corresponding solution $\mathbf{u}^1$ and check for convergence i.e. $\|\|g(\mathbf{u}^1)\|\| < TOL$. If yes, end; otherwise, set $(\mathbf{u}^0, \boldsymbol{\varepsilon}^0) \leftarrow (\mathbf{u}^1, \boldsymbol{\varepsilon}^1)$ and go to 2.

Results

As it has already been pointed out above, one of the very key points is how to choose the stepsize α in order to only allow feasible solutions, meaning $\varepsilon_{low} \leq \varepsilon_i \leq \varepsilon_{high}$. This can be done by projecting the solution back into the $[\varepsilon_{low}, \varepsilon_{high}]^n$ box at every iteration of the optimization process. However this does not guarantee that the final solution is binary. One of the very nice things of this $1d$ bandgap problem is that it has already been seen that, at least in an infinite setting, a periodic binary pattern would be a solution.

Figure 4-11 shows the optimized structure, after just 1 iteration process using the Adjoint Method, having picked α to be the largest possible but only allowing for feasible solutions. We can observe that, for this particular problem, what the optimization wants to find is two kind of directions: firstly, the one that gives the optimal pattern (meaning the 'kind of' periodicity that we expect), and the other one is just pushing apart all permittivities as much as possible. That is, it wants to maximize contrast, once it has found the discrete pattern we look for. When trying to find the optimal pattern for the sought solution the objective function behaves, at least locally, in a convex way and thus the linesearch[2] for α makes all the sense. That is, $h(\alpha) = g(\mathbf{u}, \boldsymbol{\varepsilon} + \alpha\boldsymbol{\varepsilon})$ is locally convex and when minimizing h over α, obtaining α such that $h'(\alpha) = 0$ can be easily done. However, when the direction points towards maximizing the contrast within the $\boldsymbol{\varepsilon}$ on different elements there would never be an end, meaning we would like to pick the largest α possible, determined by the bound on $\boldsymbol{\varepsilon}$. We would often find a combination of both kind of directions in which to move and thus the optimal α to choose must consider all these situations.

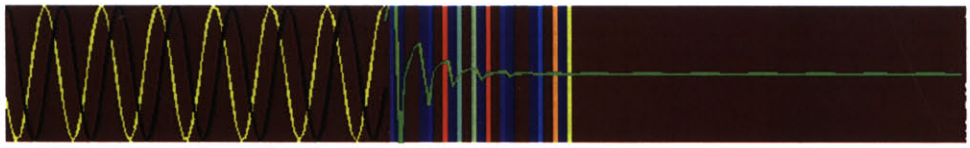

Figure 4-11: Case corresponding to $\varepsilon_i \in [\varepsilon_{low}, \varepsilon_{high}]$. Solution patterns, in black the left traveling incoming wave, in yellow the reflected and in green the transmitted.

Figure 4-14 shows the next iteration ε as well as the reflection rate with respect to the frequency. The frequency chosen corresponds to $\omega = 0.33423$ once normalized over the period, which is the ω_2 of total transmission in previous sections. The non-unitary value of it is $\omega = 11$.

The only negative aspect about the obtained solution is the fact that in general it is not binary. One could think on just projecting all solutions inside the box constraint into the closest value, either ε_{low} or ε_{high}. The solution might be much worse but one

[2]There is not a deep analysis of the linesearch process here. Further discussions can be found, for instance, in [1]

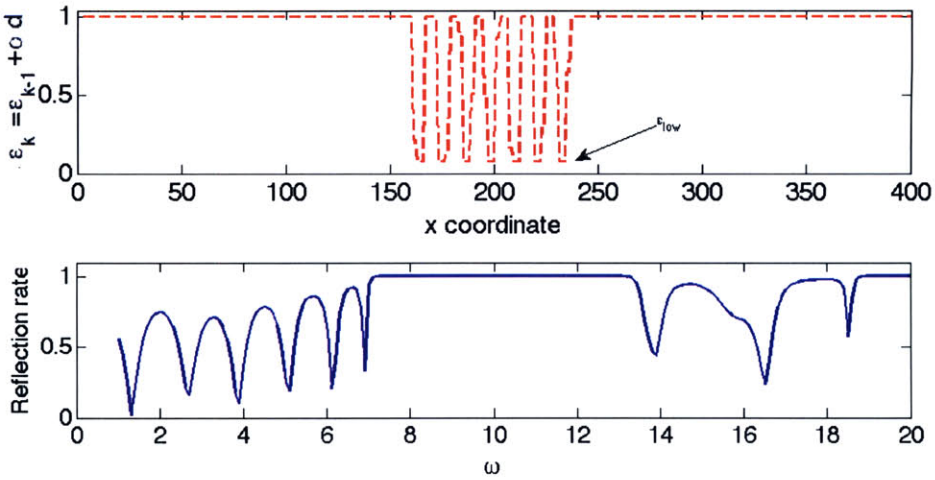

Figure 4-12: Projected into the binary box $\varepsilon_i \in \{\varepsilon_{low}, \varepsilon_{high}\}$ case. Top: Next iteration $\boldsymbol{\varepsilon}$ using the Adjoint Descent Direction and the optimized α. Bottom: Reflection versus ω plot.

could think that if we do not stop the optimization and continue with the iterations we might improve the results. However that is not the case. Once all values of the permittivity have been projected into the valid binary values the solution has a periodic-like pattern which will never be removed since the predominant direction found by the Adjoint method would just want to increase the contrast between the values, and that is not allowed. The only solution would be to start from scratch with a new initial guess.

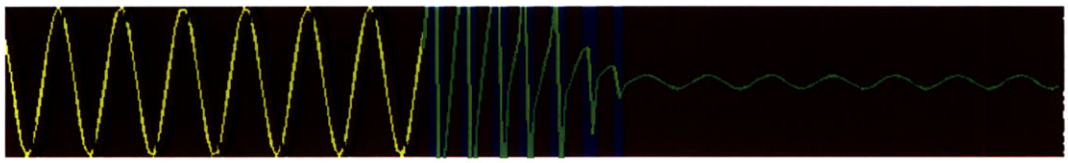

Figure 4-13: Projected into the binary box $\varepsilon_i \in \{\varepsilon_{low}, \varepsilon_{high}\}$ case. Solution patterns, in black the left traveling incoming wave, in yellow the reflected and in green the transmitted. .

Figure 4-13 shows the solution for the previous case when all permittivities are chosen binary (some more iterations have been carried out without any improvement at all). Moreover, figure 4-14 shows the new ε picked (all in just 1 iteration) and

the reflection versus ω pattern to show the size of the first bandgap, which has been noticeably reduced from the one in the previous case. The transmission coefficient after the first kind of optimization corresponds to an order 10^{-6} whereas for the solution in figure 4-13 it increases up to 10^{-2} due to the full projection into the extrema of the permittivities.

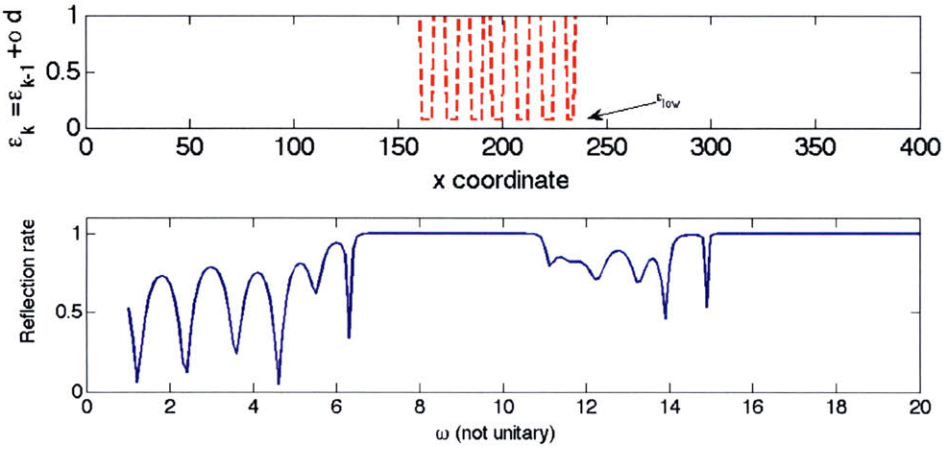

Figure 4-14: Projected into the binary box $\varepsilon_i \in \{\varepsilon_{low}, \varepsilon_{high}\}$ case. Top: Next iteration $\boldsymbol{\varepsilon}$ using the Adjoint Descent Direction and the optimized α. Bottom: Reflection versus ω plot.

Chapter 5

Conclusions and Future Research

This chapter sums up the main conclusions that must be taken out of the research carried out and introduces some future and forthcoming lines of research. As it has already been mentioned multiple times in the previous sections, this field of research is quite new and therefore a lot of work still needs to be done.

5.1 Conclusions

The work that has been presented in this thesis can really be seen as a first step in this new field, the metamaterial design. It is actually the new material science that leads all of us to think a little bit beyond classic materials. In fact, metamaterials will provide a great deal of new opportunities and possibilities. We will soon be able to filter nonlinear shocks, create flat lenses, hide objects from our eyes and ears,... etc.

One can actually think that this new filed consists of three ingredients, two of which have been covered in this text for some of the applications in the linear regime. The first step is to be able to accurately simulate the materials we are designing. The second one is to optimize them in order to provide the interesting properties we are looking for. The third and last one but not least is actually manufacturing all these materials.

Although the reader might think that it is all about building and manufacturing,

the importance of simulation and optimization can not be underestimated. Firstly because we are generating patterns with very particular properties due to its internal structure, and in most of the cases, small changes in such structure may lead to huge modifications of the aimed property. Furthermore, one can seldom find patterns that can be easily thought. As it has been already mentioned before, some physical intuition has led to the discovery of some highly interesting patterns but this is no longer valid for more sophisticated structures and even less valid when we think of finite structures (which are actually the ones that will be manufactured). That is, most physically derived materials assume infinite periodicity and thus, when manufactured and such periodicity is lost, the properties will, most likely, be also lost.

It is therefore clear that in order to find the finite patterns that still provide a certain property, some optimization must be carried out. The optimal control optimization used successfully for the one dimensional bandgap problem defines the path to follow. Although some problems can be carefully formulated in terms of eigenvalues and there the optimization works well, in general most metamaterial optimization problems can only be formulated as an optimal control problem. Such optimization provides finite and optimal structures and patterns satisfying the sought characteristic. We definitely need reliable optimization in order to obtain the very nonintuitive patterns forming most metamaterials.

We also need to point out that simulations play a very important role. In fact, whenever we move into the nonlinear world, as introduced in the next section, shock waves will need to be treated and therefore, if accurate solutions are sought, high-order methods capturing the shocks will also be required. The Hybridizable Discontinuous Galerkin method turns up to be a very good solution for that.

Still we are not done yet. Some of the optimal solutions provided by the techniques explained within this thesis will not be manufacturable. The reason for that is basically that we are still not able to manufacture patterns which are not arc-connected in two or three dimensions, especially when the background material is air. Moreover, some of the optimization techniques described above (the Adjoint approach, for instance) are actually relaxing the binary constraint due to the difficulty of dealing

with it, as it has been further explained in more detail in section 3.2. There is also the need of cleverly projecting the, likely obtained, grey solution into a black and white setting since we are only interested in using either one or another. These two issues will also be introduced in the future work section regarding Robust Optimization.

To wrap up and conclude, metamaterials' science is offering us a whole brand new world of chances and possibilities and we will only be able to take the most out of it once we can accurately simulate the phenomena, which will allow us to perform an effective binary optimization, which will lead at the same time to manufacturable patterns. After that, we will just enjoy and take advantage of such metamaterials.

5.2 Lines of future research

Metamaterials' design is quite a new topic and thus a lot of research needs still be carried out. There is also a very wide range of applications and some of them might require a very particular analysis but the work on this thesis tries to provide a quite general point of view by proposing, in particular, a method based on optimal control optimization. So, we really focus on this perspective, issues might arise either when optimizing or when simulating. After that, one must conclude whether the designed material is manufacturable or not and therefore some manufacturability constraints will also show up as important topics of future work.

On the one hand, we can really think on further applications beyond the wave equation, such as the heat equation or the negative Poisson's ratio problem. We can also consider linear and/or nonlinear elastic materials as well as how waves are propagated throughout them. Similar problems can also be thought for the shallow waters equations if we seek to simulate wave propagation in such conditions: say we want to find a pattern of columns so that some transversal waves (or others) go through and some others do not, the interesting idea of invisible ports.

If we think of manufacturability, it will also be essential to solve the equivalent problems but in 3d. Extension to higher dimensions is also a required future work. Some particular problems might just need to be solved in slabs or plates, i.e. basically

a 3d case but with one direction much smaller than the other two and constant. Examples and interesting applications can easily be found in all these scenarios and thus research on the extension of the ideas here presented need to be done.

However, the future work just described is something we already knew: since this is a new topic we are just giving here the first approximations for low dimensional cases where some complicated issues already arise but such extensions have always been considered. Beyond them, there are also some other issues that we will also need to face in the future and that only arise because of the particularity of this science: Robust Optimization providing really manufacturable materials and some non-intuitive extensions to nonlinear equations. They are both carefully analyzed in the next and last two subsections.

5.2.1 Nonlinearities

The wave equation analyzed within this thesis as well as the elastic equations for the negative Poisson's ratio and the heat equation for the heat transfer problem are all linear. We say that a Partial Differential Equation is linear when any linear combination of solutions is still a solution in the homogeneous case. Such equations describe a large amount of phenomena. Moreover, everything turns up to be quite simple due to the fact that the PDE discretization results in a linear system of equations as in (5.1). The boundary conditions and external forcing define $\mathbf{f}$ whereas A is given by the discretization of the problem.

$$A\mathbf{u} = \mathbf{f} \tag{5.1}$$

Nevertheless, a much wider range of applications can just be modeled through nonlinear equations. Whenever we move into the nonlinear world the previous linear system of equations turns up to be nonlinear and thus a Newton-Raphson method will be required in order to solve it. If this was the only difference we could still easily extend all our results from the linear regime to the nonlinear. The space of solutions to the homogeneous system of PDEs will no longer be a vector space and, for instance

in the wave equation, there is no such idea as frequency.

So first of all, the time dependent wave equation needs to be implemented and used since the solutions do no longer satisfy the superposition principle. Furthermore, nonlinear equations might create shocks or discontinuities in the solution, which will really complicate the usage of high order. Moreover, the optimization problem will not be able to be formulated in terms of a linear system of equations defined by the PDE unless it is linearized, which would clearly be a new source of error.

Some of the equations that will be used for the simulation of some common nonlinear wave propagation phenomena will often bring the nonlinearities up from a non-constant propagation speed $c = c(u)$. The Burger's equation is the nonlinear extension of the 1st order wave equation but using the actual solution as propagation speed ($c(u) = u$) instead of a constant c. This equation will show up quite often when dealing with fluids: the sonic boom created by an airplane crossing the sound speed barrier propagation throughout air is modeled by the Burger's equation, for instance. The Korteweg-de Vries or just KdV equation models waves on shallow waters surfaces. Solitons are wave pulses that travel quite isolated and they can be modeled through the KdV equation. Nonlinear elasticity formulations need also to be used under large deformations. Below here we can see some of the nonlinear wave equations that we will need to consider in future projects.

$\frac{\partial u}{\partial t} + u\nabla u = 0$	Burger's Equation	Sonic Boom
$\frac{\partial u}{\partial t} + \frac{\partial^3 u}{\partial x^3} + u\frac{\partial u}{\partial x} = 0$	1d KdV Equation	Solitons
$\frac{\partial}{\partial x}\left(\frac{\partial u}{\partial t} + u\frac{\partial u}{\partial x} + \varepsilon^2\frac{\partial^3 u}{\partial x^3}\right) + \lambda\frac{\partial^2 u}{\partial y^2} = 0$	Kadomtsev-Petviashvili Eq.	2d for KdV
$\frac{\partial^2 u}{\partial t^2} + c(u)\nabla^2 u = 0$	c(u) Wave Equation	Multiple apps

So what are the kind of metamaterials' applications that one can find within the nonlinear wave propagation regime? There are actually a bunch of them and, in fact, there are for sure a lot more of which no-one has ever thought yet. One of the many applications in which we can think is the nonlinear wave dispersive material. Elastic

materials satisfy a $\sigma = E\varepsilon$[1] relation in the 1d linear regime, which corresponds to a small deformation. In higher dimensions and for elastic solids the Poisson's ratio must also be considered and the relations between the vector of strains and the vector of stresses is still linear. However, whenever we move into a larger deformation regime the relation between σ and ε is no longer linear. Classic materials often behave quite symmetrically, meaning that the $\sigma - \varepsilon$ plot is symmetric with respect to the origin and thus the material behavior under positive tension is equivalent but with the sign flipped to the behavior under compression. It might be of interest to be able to design a material which is able to perform a very different reaction for a positive tension and compression, as shown in figure 5-1.

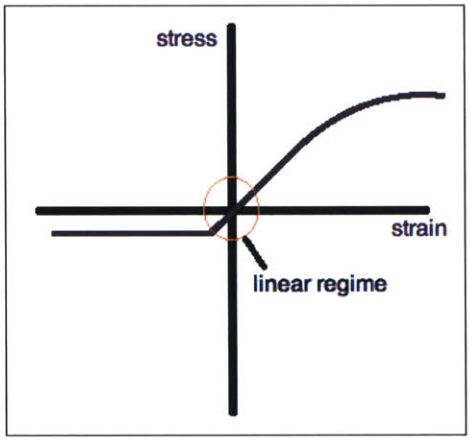

Figure 5-1: Strain-stress diagram for the dispersive metamaterial

In the end, the clever binary combination of two materials of different stiffnesses and elastic properties might lead to a material which is able to filter out (in terms of dispersion and not dissipation) some undesired nonlinear effect whereas any linear wave would still propagate normally. This materials would allow us to transform a large amplitude nonlinear pulse into an incoherent train of small amplitude waves that will no longer be an issue for the receiver. C. Daraio et al. have been doing some experimental work and performing genetic algorithms-based optimization on granular structures and have actually been able to find some structures reducing nonlinear effects noticeably, see [15, 18].

[1]Note that σ represents the stresses, ε the strains and E the Young's modulus

In a similar field and also based in a granular model[2] the same team of researchers has also carried out some nice work on sound bullets. This is actually designing a metamaterial throughout which acoustic waves propagate in such a way that after a certain determined distance such waves collapse producing a shock. Figure 5-2 is taken from [53] and describes the context of this application.

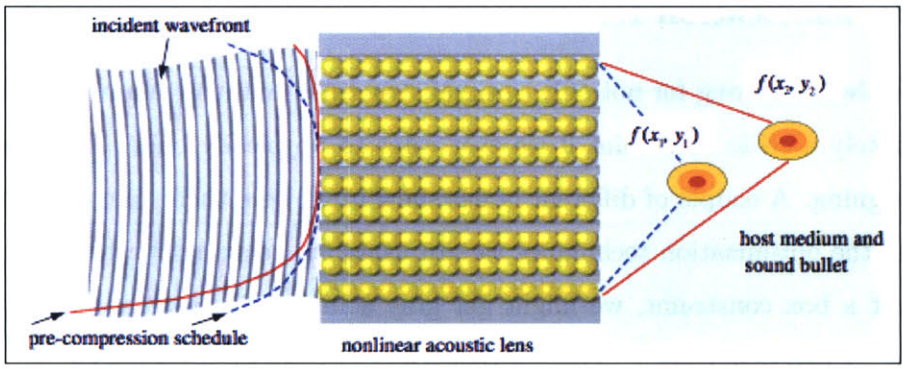

Figure 5-2: Sound bullets approach taken from A. Spadoni and C. Daraio in [53]

It would also be interesting to be able to design a small material capable of filtering out any nonlinear acoustic wave large amplitude pulse without perturbing the linear ones.

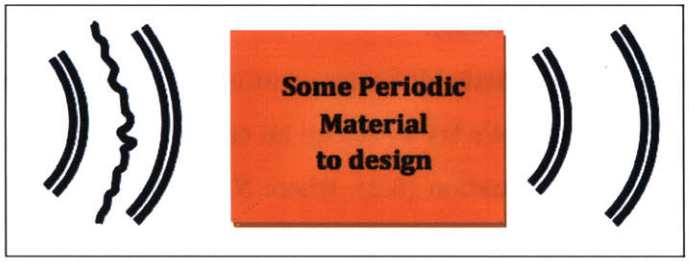

Figure 5-3: Schematic analysis of the Passive Hearing Acoustic protection

This metamaterial could be used as an earplug and would not affect any normal sound (music, voice... reasonable loudness) while dispersing all large pulses due to explosions or other kind of sonic booms. Figure 5-3 shows the schematic idea of how this earplugs would work.

[2]Granular meaning that the shape of the materials are fixed and either the material, the dimensions or the position are tuned cleverly.

To sum up, a bunch of different new applications could be efficiently solved if we were able to perform high accurate simulations and efficient optimization also on nonlinear problems. All the situations described here are just a little taste of what could potentially be achieved.

5.2.2 Fabrication Robustness

We are always looking for not only optimal structures but also manufacturable. This is definitely a critic constraint if we ever want to physically build the materials we are designing. A couple of different issues show up in here then: first of all and since most of the optimization techniques we are using are relaxing the binary constraint into just a box constraint, we might get gray solutions in between and clearly not necessarily two materials.

Lord Rayleigh observed back in 1887 that Photonic Crystals would always tend to separate the pattern into two materials with properties as different as possible[3]. However there is no way this is also going to happen in all other situations. Moreover, we might get non arc-connected patterns in 2d or 3d which would not really be manufacturable if the background material is, as often, air (things do not fly or float in air by themselves in real world).

In order to understand a little bit better what is going on and what we really mean by Fabrication Robustness let's try to set up an easy example. Say we are interested in solving the problem in equation (5.2), where $S \in \mathbb{R}^n$ and $f : \mathbb{R}^n \to \mathbb{R}$ is a convex function.

$$\begin{aligned} z^* = \min_x \quad & f(x) \\ \text{s.t.} \quad & x \in S \end{aligned} \tag{5.2}$$

The idea of *fabrication robustness* has to do with the concern that, even if the data and algorithms are accurate, the actual solution to the optimization problem z^* might not be manufacturable as explained above. It might be because of technological

[3]This is not magic. It can be shown that maximizing the distance between eigenvalues produces such a result, see for instance [19]

limitations or even human factors but say that we can really not build the optimal solution z^*. All in all, we are interested in finding a close solution constrained to be manufacturable, paying the minimum price on the objective function optimal value. So, in the end, we want to find a robust optima: an optima such that any 'close enough'[4] point (say there is one, at least, manufacturable) does not worsen a lot the optimal value. Equation (5.3) shows the optimization problem that computes the worst possible solution from all those 'close enough' to a given feasible solution $x \in S$. Say then that $\delta > 0$ is some prescribed distance in a given norm $||\cdot||$.

$$\begin{aligned} \hat{f}_\delta(x) = \max_y \quad & f(y) \\ \text{s.t.} \quad & ||y - x|| < \delta \\ & y \in S \end{aligned} \tag{5.3}$$

We are interested in finding a minimum of f over a set of points making sure that all 'close enough' neighbors are good enough. Therefore we can say then that $\hat{f}_\delta$ is the robust version of initial objective function f and it is actually this function $\hat{f}_\delta$ the one that is to be optimized. To sum up we will solve(5.4) instead of (5.2).

$$\begin{aligned} z^*_\delta = \min_x \quad & \hat{f}_\delta(x) \\ \text{s.t.} \quad & x \in S \end{aligned} \tag{5.4}$$

Let's see a simple example. Say you are flying over Mt. Elbert, Colorado and want to drop some kind of device in the highest point possible. You might think that throwing it to the peak should be the best idea but since the slope of the mountain around the peak is much sharper and there is a real chance of error (assume that it is controlled and bounded by 50m from where you are pointing), you should actually point to some other region where, although it is not as high as the actual peak, the whole big region is quite high in average.

In this case we want to maximize $f(x, y)$ ='height at coordinate point (x, y)'. Figure 5-4 shows the countours of $f(x, y)$, and $\hat{f}_{\delta=50}(x, y) = \min_{(x,y)}$'height of any

[4]The concept 'close enough' later described by δ basically allows a certain number of pixel changes from one material to another according to a norm defined for that purpose.

point in the 50m circle around (x, y). Note the difference between the optima for both functions.

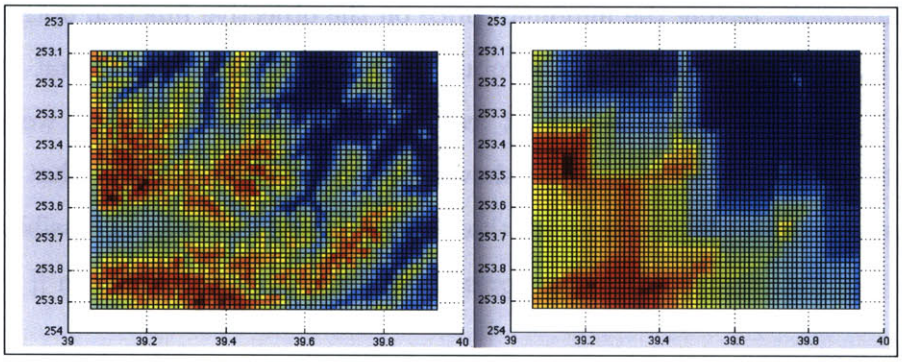

Figure 5-4: Left: Contour plot of the Mt. Albert; Right: Contourplot of the robust version of the Mt. Albert. Axis indicate parallel and meridian degrees

The same scenario is now shown for an easier fake mountain. Imagine the profile of this Mt. Fake looks like the one shown in figure 5-5, which is actually the superposition of a modified sine and a gaussian pulse. There the peak is clearly on the top of the gaussian but if we solve the robust version, assuming a large enough δ (Note that $\delta = 0$ actually would imply that $\hat{f}_\delta = f$) the robust peak of Mt. Fake is no longer at the (x, y) position corresponding to the gaussian center.

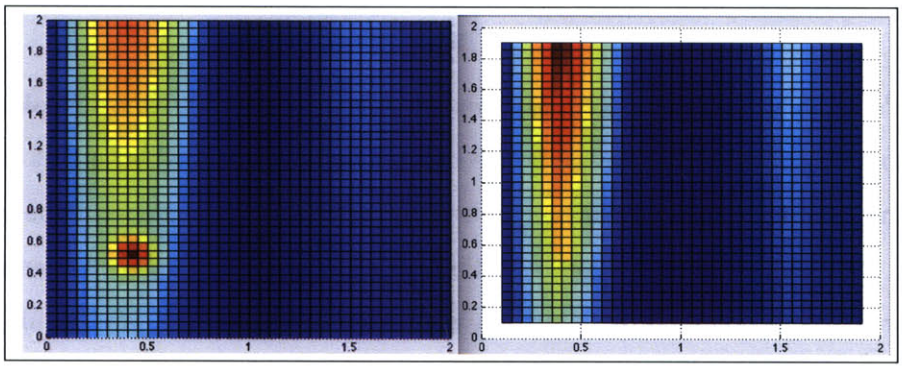

Figure 5-5: Left: Contour plot of the Mt. Fake; Right: Contourplot of the robust version of the same function.

This research is nowadays being carried out by R.M Freund et al. in [16] and will be a key extension to all the optimization techniques developed in this thesis and also for any further algorithms for both linear and nonlinear metamaterials' design.

Bibliography

[1] Dimitri P. Bertsekas. *Nonlinear Programming.* Athena Scientific, 2008.

[2] Y. Cao, S. Li, L. Petzold, and R. Serban. Adjoint sensitivity analysis for differential algebraic equations: The adjoint dae system and its numerical solution. *SIAM J. Sci. Comput*, 24(3):1076–1089, 2003.

[3] B. Cockburn, B. Dong, and J. Guzmán. A superconvergent ldg-hybridizable galerkin method for second-order elliptic problems. *Math. Comp.*, 77:1887:1916, 2008.

[4] B. Cockburn, B. Dong, and J. Guzmán. A hybridizable and supercovergent discontinuous galerkin method for biharmonic problems. *J. Sci. Comput.*, 40(1-3):141–187, 2009.

[5] B. Cockburn, B. Dong, J. Guzmán, M. Restelli, and R. Sacco. A hybridizable discontinuous galerkin method for steady-state convection-diffusion-reaction problems. *SIAM J. Sci. Comput*, 31(5):3827–3846, 2009.

[6] B. Cockburn and J. Gopalakrishnan. A characterization of hybridized mixed methods for second order elliptic problems. *SIAM J. Numer. Anal.*, 42(1):283–301, 2004.

[7] B. Cockburn, J. Gopalakrishnan, and R. Lazarov. Unified hybridization of discotinuous galerkin, mixed and continuous galerkin methods for second order elliptic problems. *SIAM J. Numer. Anal.*, 47:1319–1365, 2009.

[8] B. Cockburn, J. Gopalakrishnan, and F.J. Sayas. A projection-based error analysis of hdg methods. *Math. Comp.*, To appear.

[9] B. Cockburn, J. Guzmán, and H. Wang. Superconvergent discontinuous galerkin methods for second-order elliptic problems. *Math. Comp.*, 78:1–24, 2009.

[10] B. Cockburn and C. W. Shu. The local discontinuous Galerkin method for convection-diffusion systems. *SIAM J. Numer. Anal.*, 35:2440–2463, 1998.

[11] B. Engquist and A. Majda. Absorbing boundary conditions for the numerical simulation of waves. *Mathematics of Computation*, 31:629–651, 1977.

[12] R.M. Errico. What is an adjoint model? *Bulletin Am. Meteorogical Soc.*, 78:2577–2591, 1997.

[13] K.E. Evans, M.A. Nkansah, and I.J Hutchinson. Modelling negative poisson ratio effects in network-embedded composites. *Acta metall. mater.*, 40(9):2463–2469, 1992.

[14] Mohamed Farhat, Sebastien Guenneau, Stefan Enoch, and Alexander B. Movchan. Cloaking bending waves propagating in thin elastic plates. *Phys. Rev. B*, 79, 2009.

[15] F. Fraternali, M.A. Porter, and C. Daraio. Optimal design of composite granular protectors. *Mechanics of Advanced Materials and Structures*, 17:1–19, 2010.

[16] R. M. Freund, N. C. Nguyen, J. Peraire, Joel Saa-Seoane, and H. Men. Fabrication robustness. March 2011.

[17] Allan Greenleaf, Yaroslav Kurylev, Matti Lassas, and Gunther Uhlmann. Cloaking devices, electromagnetic wormholes, and transformation optics. *SIAM Review*, 51(1):3–33, 2009.

[18] E.B. Herbold, J. Kim, V.F. Nesterenko, S. Wang, and C. Daraio. Tunable frequency bandgap and pulse propagation in a strongly nonlinear diatomic chain. *Acta Mechanica*, 205(1-4):85–103, June 2009.

[19] John D. Joannopoulos, Steven G. Johnson, Joshua N. Winn, and Robert D. Meade. *Photonic crystals: molding the flow of light.* Princeton Univ. Press, 2008.

[20] C. Johnson and J. Pitkaranta. An analysis of the discontinuous galerkin method for a scalar hyperbolic equation. *Mathematics of Computation*, 46(173):1–26, 1986.

[21] Steven G. Johnson. Notes on adjoint methods for 18.336. MIT course 18.336 material support.

[22] Steven G. Johnson. Notes on perfectly matched layers (pmls).

[23] Robert V. Kohn, Daniel Onofrei, and Michael I. Weinstein. Cloaking via change of variables for the helmholtz equation. *Communications on Pure and Applied Mathematics*, LXIII:0973–1016, 2010.

[24] Roderic Lakes. Foam structures with a negative poisson's ratio. *Science*, 235:1038–1040, February 1987.

[25] Roderic Lakes. Deformation mechanisms in negative poisson's ratio materials: structural aspects. *Journal of materials science*, 26:2287–2292, 1991.

[26] J. Löfberg. Yalmip : A toolbox for modeling and optimization in MATLAB. In *Proceedings of the CACSD Conference*, Taipei, Taiwan, 2004.

[27] H. Men, NC Nguyen, RM Freund, PA Parrilo, and J. Peraire. Bandgap optimization of two-dimensional photonic crystals using semidefinite programming and subspace methods. *Journal of Computational Physics*, 229:3706–3725, 2010.

[28] H. Men, NC Nguyen, RM Freund, K. M. Lim, PA Parrilo, and J. Peraire. Design of photonic crystals with multiple and combined band gaps. *Phys. Rev. E*, Submitted.

[29] Niels A. Mortensen, Ole Sigmund, and Olav Breinbjerg. Prospects for poorman's cloaking with low-contrast all-dielectric optical elements. *Journal of the European Optical Society*, 4, 2009.

[30] Hoai-Minh Nguyen. Cloaking via change of variables for the helmholtz equation in the whole space. *Communicatinos on Pure and Applied Mathematics*, LXIII:1505–1524, 2010.

[31] N.C. Nguyen and J. Peraire. Hybridizable discontinuous Galerkin methods for partial differential equations in continuum mechanics. *International Journal of Numerical Methods in Engineering*, Submitted.

[32] N.C. Nguyen and J. Peraire. A shock-capturing hdg method for CFD applications. *J. Comput. Phys.*, Working Paper.

[33] N.C. Nguyen, J. Peraire, and B. Cockburn. An implicit high-order hybridizable discontinuous Galerkin method for linear convection-diffusion equations. *J. Comput. Phys.*, 228:3232–3254, 2009.

[34] N.C. Nguyen, J. Peraire, and B. Cockburn. An implicit high-order hybridizable discontinuous Galerkin method for nonlinear convection-diffusion equations. *J. Comput. Phys.*, 228:8841–8855, 2009.

[35] N.C. Nguyen, J. Peraire, and B. Cockburn. A comparison of HDG methods for Stokes flow. *Journal of Scientific Computing*, 45:215–237, 2010.

[36] N.C. Nguyen, J. Peraire, and B. Cockburn. A hybridizable discontinuous Galerkin method for Stokes flow. *Comput. Methods Appl. Mech. Engrg.*, 199:582–597, 2010.

[37] N.C. Nguyen, J. Peraire, and B. Cockburn. A hybridizable discontinuous Galerkin method for the incompressible Navier-Stokes equations. In *Proceedings of the 48th AIAA Aerospace Sciences Meeting and Exhibit*, pages AIAA Paper 2010–362, 2010.

[38] N.C. Nguyen, J. Peraire, and B. Cockburn. Hybridizable discontinuous Galerkin methods. In J. S. Hesthaven and E. M. Ronquist, editors, *Spectral and High Order Methods for Partial Differential Equations*, volume 76, pages 63–84, 2011.

[39] N.C. Nguyen, J. Peraire, and B. Cockburn. An implicit high-order hybridizable discontinuous Galerkin method for the incompressible Navier-Stokes equations. *J. Comput. Phys.*, 230:1147–1170, 2011.

[40] N.C. Nguyen, J. Peraire, and B. Cockburn. Implicit high-order hybridizable discontinuous Galerkin methods for acoustics and elastodynamics. *J. Comput. Phys.*, Accepted.

[41] N.C. Nguyen, J. Peraire, and B. Cockburn. Hybridizable discontinuous Galerkin methods for the time-harmonic Maxwell's equations. *J. Comput. Phys.*, Submitted.

[42] Ardavan F. Oskooi, David Roundy, Mihai Ibanescu, Peter Bermel, J. D. Joannopoulos, and Steven G. Johnson. MEEP: A flexible free-software package for electromagnetic simulations by the FDTD method. *Computer Physics Communications*, 181:687–702, January 2010.

[43] P. A. Parrilo and S. Lall. Semidefinite programming relaxations and algebraic optimization in control. *European Journal of Control*, 9(2-3):307–321, 2003.

[44] J. B. Pendry. Negative refraction makes a perfect lens. *Phys. Rev. Lett.*, 85(18):3966–3969, Oct 2000.

[45] J. B. Pendry, D. Schurig, and D. R. Smith. Controlling electromagnetic fields. *Science*, 312:1780–1782, 2006.

[46] J. Peraire, N.C. Nguyen, and B. Cockburn. A hybridizable discontinuous Galerkin method for the compressible Euler and Navier-Stokes equations. In *Proceedings of the 48th AIAA Aerospace Sciences Meeting and Exhibit*, pages AIAA Paper 2010–363, 2010.

[47] Raul Radovitzky. Summit finite element method solver for elasticity.

[48] Lord Rayleigh. On the maintenance of vibrations by forces of double frequency, and on the propagation of waves through a medium endowed with a periodic structure. *Philosophical Magazine*, 24(147):145–159, 1887.

[49] Benjamin Recht, Maryam Fazel, and Pablo A. Parrilo. Guarranteed minimum-rank solutions of linear matrix equations via nuclear norm minimization. Preprint, February 2008.

[50] Joel Saa-Seoane. Hexagonal lattices in 2d photonic crystals. line defects, waveguides and high transmission 60 degrees bends. Course project for MIT 18.369, 04 2010.

[51] Joel Saa-Seoane. Analysis and simulation of auxetic-elastic metamaterials providing an effective negative poisson's ratio. Course project for MIT 16.225, May 2011.

[52] S.C. Soon, B. Cockburn, and H. K. Stolarski. A hybridizable discontinuous galerkin method for linear elasticity. *International Journal of Numerical Methods in Engineering*, 80(8):1058–1092, 2009.

[53] A. Spadoni and C. Daraio. Generation and control of sound bullets with a nonlinear acoustic lens. *Proc Natl Acad Sci USA*, 107(7230), 2010.

[54] K.C. Toh, M.J. Todd, and R.H. Tutuncu. Sdpt3 — a matlab software package for semidefinite programming. *Optimization Methods and Software*, (11):545–581, 1999.

[55] Hui Wan, Hideyuki Ohtaki, Shinya Kotosaka, and Guoming Hu. A study of negative poisson's ratios in auxetic honeycombs based on a large deflection model. *European Journal of Mechanics A/Solids*, 23:95–106, 2004.

[56] D.U. Yang, S Lee, and F.Y. Huang. Geometric effects on micropolar elastic honeycomb structure with negative poisson's ratio using the finite element method. *Finite Elements in Analysis and Design*, 39:187–205, 2003.